Utrecht University

UTRECHT UNIVERSITY
MSC CLIMATE PHYSICS
INSTITUTE FOR MARINE AND ATMOSPHERIC RESEARCH UTRECHT

AMOC variability, a key factor in emission reduction scenarios

Author:
J.M. Valentí Muelas [6515886]

Supervisor:
Prof. Dr. Ir. H.A. Dijkstra

June 2020.

Contents

Abstract

The climate system response to emission reduction shows time dependencies when evaluated in terms of global mean surface temperature (GMST). The Atlantic meridional overturning circulation (AMOC) variability may be forcing a non-linear behaviour on GMST response to emission reduction. In this study, emission reduction is evaluated with eight starting actions times on three equilibrium climate sensitivities (ECS), using the PLASIM-GENIE intermediate complexity Atmosphere and Ocean global climate model. Under these CO_2 reducing scenarios, AMOC collapses in six out of the twenty-four simulations performed. The effect of the AMOC collapse in the emission reduction scenarios is a transient faster response (cooling) in the short term compensates with a slower response to emission reduction in the forthcoming decades. In non-collapsing scenarios, the emission reduction response might have initial conditions dependencies with the AMOC variability.

1 Introduction

Anthropogenic climate change is a global concern that can be slowed down and even reversed by implementing the necessary measures. The human mark on our planet is found without a doubt in many features of the Earth's climate. Since preindustrial times, global temperature records follow the anthropogenic GHGs emissions growing trends and cannot be explained in any way by a natural climate variation alone (Rosenzweig et al., 2008). Besides global temperatures, the ocean heat content (OHC) is also rapidly increasing at an unprecedented rate, which can only be explained by anthropogenic emissions contribution (Barnett et al., 2001). Moreover, global warming also leads to changes in the water cycle (e.g. precipitation, hydrological systems and snow cover) and can even lead to tipping points (e.g. the AMOC collapse (Lenton et al., 2008) or the melting of Greenland's ice sheet (Noël et al., 2017)).

Global annual GHGs emissions continue to rise yearly, having reached 33GT of CO_2 emitted in 2019. However, some Western countries have been already for more than ten years reducing their emissions (Commission and Agency, 2020). They are trying to follow the decrease in emissions proposed in the Paris Agreement (Le Quéré et al., 2018). Although not at a rapid pace, many countries have been investing in renewable energies, intending to reduce the impact on the environment. Nowadays, renewable energies add up to 24% of the electricity production share globally. China, together with the US, are the countries with the highest production in renewable energies, but despite their investment, they are still the two countries with the highest emissions of GHGs worldwide. Furthermore, other strategies aim for less contaminant processes of combustion (i.e. Carbon Capture and Storage systems), but detailed plans are still lacking (Kheshgi et al., 2012). With the above-mentioned, and the historical biggest contributors (i.e. the European Union and the US) depleting their emissions, global CO_2 annual emissions could be expected to be in a decreasing trend. However, this is not the case, as the vast majority of the World countries are in the opposite side of the spectrum and they are increasing GHGs emissions as their economy grows, contributing to the yearly growth on global emissions that continues to happen nowadays.

In the last decades, several socioeconomic based emission reduction pathways; RCP (Representative Concentration Pathway) scenarios (Van Vuuren et al., 2007; Clarke et al., 2007; Fujino et al., 2006; Riahi et al., 2011) were designed to forecast a feasible range of GHGs emission pathways. When applied in global climate models, they showed the huge difference between start

acting at different years and not acting at all. RCP scenarios give a broad spectrum of the possible climate in the forthcoming 150 years. When RCP scenarios were proposed, RCP 2.6, which forecast an early action, was seen as the perfect line of performance. However, it is already too late to try to follow the mentioned RCP 2.6 (Van Vuuren et al., 2007) as it suggests an earlier start of the emissions reduction, abatement, CO_2 absorption and mitigation strategies that we are not implementing or following yet. Despite the advice from climate scientist from the late XXth century (Grubb et al., 1999), the World's response seems to be following the Worst Scenario (Riahi et al., 2011): the RCP 8.5, that conceives a continually growing economy that burns out all the oil reservoirs rising the global mean temperature up to 12.6ºC higher than preindustrial in Coupled Model Intercomparison Project (CMIP5) models.

Additionally, new CMIP6 models suggest a possible higher climate sensitivity (ECS) that would fall in the range of 1.8-5.6ºC, exceeding 4.5ºC, in 10 out of the 27 models studied (Zelinka et al., 2020). This implies a huge difference when comparing to CMIP5, where the ECS range was of 1.5-4.5ºC (Andrews et al., 2012). Higher ECS could also force the system towards a tipping point in a shorter term than expected. A clear example of tipping point is found in the AMOC, a large system of ocean currents that as part of the global thermohaline circulation carries warm water from tropical latitudes northwards into the North Atlantic. The AMOC plays an important role in the climate system. Paleo-climate records from Greenland ice cores revealed repeated rapid transitions between cold and warmer states of the climate (McManus et al., 2004). This transitions may be the result of a gradual decrease of the AMOC up to a tipping point when the circulation collapses and induces the rapid change in the climate system (Rahmstorf, 1996; Rahmstorf et al., 2005).

The main goals of this study are: (i) to quantify and better understand the starting-time dependencies of the Earth system response to emissions reduction and (ii) to evaluate the AMOC tipping behaviour under different ECS. In Boucher et al. (2012) they described a starting-time dependency in an Earth system model under a CO_2 concentration reducing at a fixed rate of $1\%\ year^{-1}$. They found an initial conditions dependent lag in the GMST response to emissions reduction, with increasing time lag for larger CO_2 concentrations. In this study, we try to find additional starting-time dependencies, by using a more plausible emission reduction scenario like the one proposed by Aengenheyster et al. (2018) and testing with a range of ECS (2.8-4,6ºC). The ECS is adjusted changing the strength of a series of climate feedbacks; due to the non-linear behaviour of climate feedbacks (Schneider et al., 1999), we expect to find a strong dependency of the ECS in the global temperature response to emission reduction scenarios. Furthermore, using a high ECS, considered by CMIP6, might push the system towards tipping points in a shorter term, showing the ECS dependencies in the AMOC tipping point behaviour.

To study these issues, we use the intermediate-complexity Earth system model PLASIM-GENIE, a model with atmosphere, ocean and sea ice dynamics, which is proven to behave very similarly to full-complexity models even with a lower spatial resolution (Holden et al., 2018). Furthermore, the carbon model used is described in section 2.1. The PLASIM-GENIE model was evaluated comparing the global temperature response and the AMOC strength under RCP 8.5 scenario resulting in a substantially consistent result with CMIP5 ensembles.

2 Methods

2.1 Carbon Cycle Model

CO_2 is a long-lived GHG not destroyed by any chemical reaction nor deposited on the earth surface. It is nonetheless redistributed within the major carbon reservoirs (ocean, land, biosphere and atmosphere), giving CO_2 a broad range of timescales to exchange from one to another. A small fraction of CO_2 is only removed by ocean-sediment interaction, weathering or burial. These last having timescales that reach the millennia (Archer et al., 2009). The carbon cycle model used for this study employs the IRF_{CO_2} (impulse response function) proposed by Joos et al. (2013). This function is obtained by computing the response to an emission pulse of CO_2 and the following redistribution of this atmospheric CO_2 within the major carbon reservoirs. Thus, the value of the IRF_{CO_2}(t) represents the fraction of the CO_2 pulse that still remains in the atmosphere at time t (Fig. 1). Because a small fraction lingers in the atmosphere for millennia, the efficiency of emission reduction will slow down after some decades.

Due to the simplification of only using a fit of the main 3 timescales, the IRF_{CO_2} function is of the form:

$$IRF_{CO_2}(t) = \mu_0 + \sum_{i=1}^{3} \mu_i \, exp\left(\frac{-t}{\tau_i}\right) \quad \text{for } 0 \leq t \leq 1000, \tag{1}$$

where, the non-dimensional coefficients μ_i, i = 1...3 represent the fraction associated to timescales τ_i, i = 1...3 and were obtained using a fit of a three-timescale exponential with constant offset optimized for a 100GtC emission pulse, under present day climate conditions; the list of parameters used is found in Table. 1. The parameter μ_0 is the fraction of the pulse that will take thousands of years to disappear from the atmosphere (Fig. 1). Although the coefficients are chosen for a 100GtC emission pulse, Joos et al. (2013) showed that using them for pulses in the range from 0-100GtC could cause a deviation of up to 1.2% in the infinitely small case. Concluding that, this model is a good approximation for smaller emission pulses. Under this assumption, our carbon cycle model is independent of the size of the emission pulse, as long as it is smaller or close to 100GtC. For larger pulses, carbon cycle-climate feedbacks would come into action, and the response in CO_2 distribution would differ significantly (Millar et al., 2017).

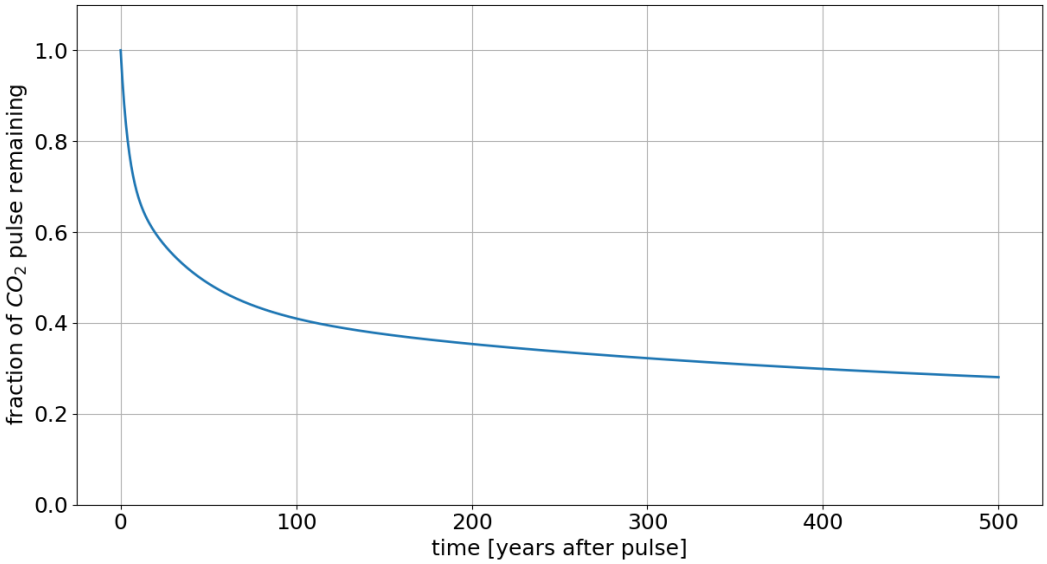

Figure 1. IRF_{CO_2} function for 100GtC size emission pulse.

In order to implement this model on emission pathways, we assume yearly global CO_2 emission to be a single pulse of emission happening in December of every year. From here, we can compute the yearly mean CO_2 concentration in the atmosphere from a given emission pathway.

$$CO_2(t) = \int_{t_0}^{t} E(t')IRF_{CO_2}(t-t')dt' + CO_2(t_0). \tag{2}$$

Here, $CO_2(t_0)$ is the preexisting carbon dioxide concentration in the atmosphere and was taken as a constant value from preindustrial levels (280 ppm).

Table 1. Coefficients to fit multi-model mean responses to a pulse emission of 100GtC

μ_0	μ_1	μ_2	μ_3	τ_1	τ_2	τ_3
0.2173	0.2240	0.2824	0.2763	394.4	36.54	4.304

2.2 Emission reduction pathways

The RCP 8.5 CO_2 emission pathway was chosen as the base emission pathway. The base emission pathway starts with 200 years at reference preindustrial CO_2 concentration of 280 ppm allowing the earth system to reach an equilibrium state before

we start testing. From there, the historical CO_2 emission data (Our World in Data) is used from 1850 up to 2010 and then the RCP 8.5 emissions (Riahi et al., 2011) is followed until the year 2200 (Fig. 2a).

In order to test the emission reduction response we draw a series of emission reduction pathways from the RCP 8.5 base scenario (Fig. 2a). The emission reduction starts from several starting years (t_s) (i.e. 2020, 2030, 2035, 2050, 2070, 2085, 2100 and 2120) following a recently used method proposed by Aengenheyster et al. (2018).

$$m(t) = \begin{cases} m_0 & t \leq t_s \\ min(m_0 + m_1(t - t_s), 1) & t > t_s \end{cases} \tag{3a}$$

$$a(t) = \begin{cases} a_0 & t \leq t_s \\ min(a_0 + a_1(t - t_s), 1) & t > t_s \end{cases} \tag{3b}$$

$$E(t) = E_0(t)(1 - a(t))(1 - m(t)) - E_n(t) \tag{3c}$$

Where, abatement (a) is an increasing share of fossil fuel energy sources that do not emit any CO_2 by capturing and storing the resulting carbon dioxide produced during the combustion. The mitigation actions (m), can be interpreted as the replacement from fossil energy to clean renewable energies such as wind, solar and hydropower and E_n represents the use of technologies directly absorbing CO_2 from the atmosphere. As E_n technologies are poorly developed nowadays, Aengenheyster et al. (2018) proposed not switching this method on, until the year 2061, when this technology could efficiently start reducing CO_2 concentrations in the atmosphere. However, in our simulations, we did not switch it on at any point as this would decrease the difference from the different reduction emission scenarios.

This reduction emission pathway can be used for different socioeconomic conditions depending on the political decisions and works by letting both m and a increase linearly until emissions are brought to zero. In our simulations we kept the parameters $a_0 = 0$ and $m_0 = 0.14$ at 2015 values (World Energy Council, 2016). For m_1 and a_1 we follow the intermediate emission reduction scenario proposed by Aengenheyster et al. (2018); The Fast Mitigation scenario, from time t_s onwards, both a_1 and m_1 have a value of 0.05, increasing the abatement and mitigation share by a 5% every year. This scenarios brings emissions to zero approximately 17 years after t_s.

Fig. 2a shows the base emission pathway with all the emission reduction scenarios for the different t_s, while Fig. 2b shows CO_2 concentrations for the different emission reduction pathways computed with IRF_{CO_2} as described in section 2.1. Furthermore, RCP 4.5, 6 and 8.5 concentration pathways given by CMIP5 models are plotted in Fig. 2b; The RCP scenarios are plotted to give an outer perspective to our emission reduction scenarios. The latest action t_s = 2120 finishes with approximately the same CO_2 concentration as RCP6 on 2200, for t_s = 2070 the CO_2 concentration matches RCP4.5 and any faster action finishes the simulation with a CO_2 concentration below RCP4.5 expectations.

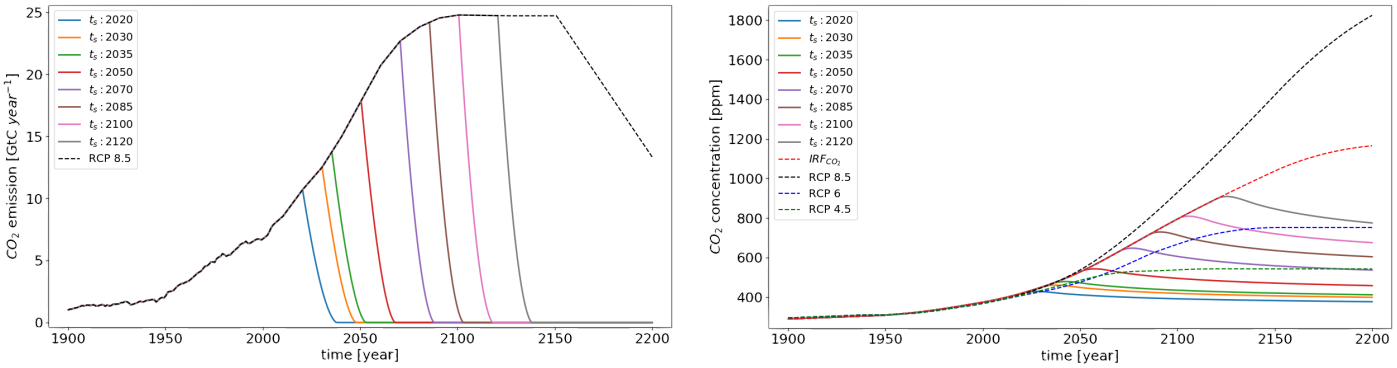

(a) (b)

Figure 2. (a) CO_2 emission pathways: Base, RCP 8.5 (black dashed) and the different t_s (solid colour lines). (b) CO_2 concentration for: the RCP 8.5, 6 and 4.5 concentration scenarios from CMIP5 (black, blue and green dashed lines), the IRF_{CO_2} from the RCP 8.5 emissions (red dashed) and the different t_s reduction emission scenarios shown in (a) are represented with the solid colour lines.

2.3 Model

PLASIM-GENIE v1.0 (Holden et al., 2016) is an Earth System Model of Intermediate Complexity (EMIC) built by coupling the Planet Simulator (PLASIM) to the ocean, sea-ice and land-surface components of the Grid-ENabled Integrated Earth system model (GENIE).

This model consist of 4 main modules. (i) PLASIM is a reduced complexity Atmosphere General Circulation Model (AGCM), with the 3-D primitive-equation Portable University Model of the Atmosphere (PUMA) at its core (Fraedrich et al., 2005).

(ii) Efficient numerical terrestrial scheme (ENTS) is a low resolution spatial model of vegetation carbon, soil carbon and soil water storage and the exchange of energy, water and carbon with the atmosphere (Williamson et al., 2006). It was originally used as land surface model for GENIE but was already implemented to PLASIM-ENTS by Holden et al. (2014).

(iii) The ocean model GOLDSTEIN is a 3-D frictional geostrophic ocean model (Edwards and Marsh, 2005). It is similar to General Circulation Models but it neglects momentum advection and acceleration.

(iv) The thermodynamic sea ice model, GOLDSTEINSEAICE also proposed by Edwards and Marsh (2005), solves the sea ice cover variations which are dependent on the net heat flux into the ice.

The coupling of these modules consists of different types: Information is shared from/to PLASIM to/from ENTS straight away every time-step. While from GOLDSTEIN and GOLDSTEINSEAICE to PLASIM it is needed two PLASIM dummy modules, one for each, at the boundaries. The coupling from PLASIM to GOLDSTEIN proceeds without the need of an extra module, and from PLASIM to GOLDSTEINSEAICE the PLASIM subroutine (ICE-SURFLUX) transforms PLASIM surface fluxes into ice fluxes, which work as input for GOLDSTEINSEAICE. The coupling of these four modules improved the performance of PLASIM considerably. However, a total of 98% of the computational effort still corresponds to PLASIM alone (Holden et al., 2016).

2.4 Climate sensitivity & Feedbacks

To calculate the equilibrium climate sensitivity (ECS) of the model we use the method proposed by Gregory et al. (2004), where we regress global and annual-mean planetary energy balance at the top of the atmosphere anomalies (R) on global and annual-mean surface air temperature anomalies (T) to obtain equilibrium climate sensitivity (ECS, x-intercept), radiative feedback (λ, regression slope) and effective radiative forcing (ERF, y-intercept), according to:

$$R = F + \lambda T \tag{4}$$

This method assumes that R can be expressed as the sum of the radiative forcing and the radiative response to a global surface temperature anomaly. As a result, we obtain a climate sensitivity of 2.77ºC for the Standard ECS runs Fig. 3a. This ECS lands slightly below the CMIP5 predicted ECS and is rather small when looking into CMIP6 ECS (Zelinka et al., 2020). However, PLASIM-GENIE was tested Holden et al. (2018) with a model ensemble with a range of ECS from 2.6ºC to 4.5ºC proving its good performance next to CMIP5. We perform a series of simulations with three different ECS; the called Standard ECS, the Enhanced ECS and the Extreme ECS simulations with climate sensitivities of 2.77, 3.76 and 4.5ºC respectively.

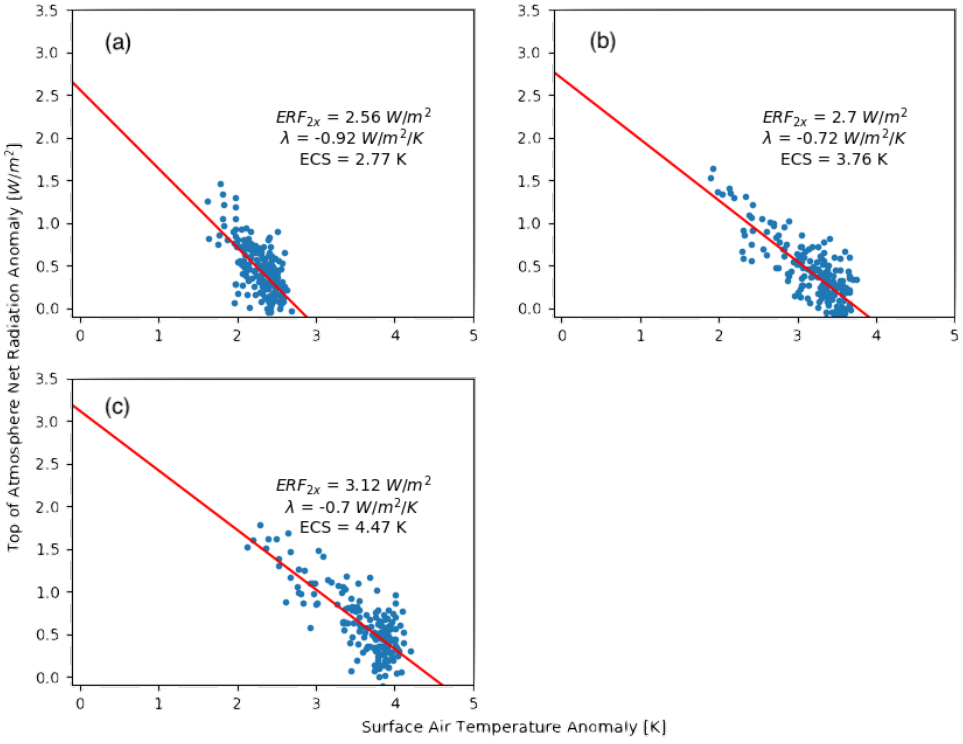

Figure 3. ECS computed with Gregory's method for Standard ECS(a), Enhanced ECS (b) and Extreme ECS (b).

PLASIM-GENIE includes several direct climate feedbacks, such as sea-ice albedo, snow albedo or water vapour, it also represents more complex feedbacks, such as atmosphere cloud dynamic or thermohaline circulation ocean feedbacks. The model cannot reproduce other dynamic ocean feedbacks, but they do not have a big influence on short term climate response, playing an important role in longer climate simulations.

To analyse the effect of feedbacks on emission reduction scenarios, we increase the ECS by increasing the strength of those feedbacks that can infer a net effect on the climate in timescales no longer than 200 years. The main feedbacks in this timescale are the water vapour and sea-ice/snow albedo feedback. In order to analyse a simpler enhanced feedback condition, we change only one parameter, the water vapour continuum absorption ($\mathcal{T}^{cont}_{H_2O}$). $\mathcal{T}^{cont}_{H_2O}$ represents about 60% of the water vapour transmissivity (Ponomarev et al., 2016) and changes in this, will directly affect upward and downward radiation fluxes in Eq. 5. We shift its value to the maximum inside the plausible ranges (Holden et al., 2014). As a result of this modified PLASIM-GENIE, we obtain an ECS of 3.76ºC for doubling CO_2 which is 1ºC above the ECS obtained in the called Standard ECS run.

Upward and downward radiation fluxes are calculated as follows:

$$F^{\uparrow LW}(z) = \mathcal{A}_S B(T_s)\mathcal{T}_{(z,0)} + \int_0^z B(T')\frac{\partial \mathcal{T}_{(z,z')}}{\partial z'}dz' \tag{5a}$$

$$F^{\downarrow LW}(z) = \int_\infty^z B(T')\frac{\partial \mathcal{T}_{(z,z')}}{\partial z'}dz' \tag{5b}$$

Where $\mathcal{T}_{(z,z')}$ are the transmissivities between level z and level z'. $\mathcal{T}$ represents the total amount of transmissivities for GHG in the atmosphere, $B(T)$ denotes the black body flux and $\mathcal{A}_s$ is the surface emissivity. $\mathcal{T}^{cont}_{H_2O}$ is defined in Eq. 6, where k_{cont} is the constant that we set to its maximum value (i.e 0.1) and u_{H_2O} is the effective amounts of water vapor. By increasing k_{cont} we increase the transmissivity of water vapour for all the radiation wave numbers, increasing the H_2O radiation absorption in the atmosphere.

$$\mathcal{T}^{cont}_{H_2O} = 1 - exp(-k_{cont}u_{H_2O}) \tag{6}$$

The net effect of increasing the value of this feedback parameter 2.5 times its original value is an ECS increase of 1ºC. The effect on climate response is described in section 2.5.

For the Extreme ECS we modified again $\mathcal{T}^{cont}_{H_2O}$ as for the Enhanced ECS, the sea-ice albedo feedback that affects directly on the net radiative forcing of the earth, is increased by shifting the maximum value of the sea ice albedo from 0.7 up to 0.75 and the critical relative humidity for stratiform clouds (rh_c) again inside the plausible ranges given by Holden et al. (2014), increasing the amount of stratiform clouds (cc_s) for higher values of relative humidity (rh) as Eq. 7.

$$cc_s = f_w\left(\frac{rh - rh_c}{1 - rh_c}\right)^2 \tag{7}$$

The higher amount of stratiform clouds for higher values of rh increases the long wave radiation absorption increasing the ECS of the system. However, with this increases in the feedback parameters, the preindustrial GMST (PI) reaches too high values ($\sim 18°C$). In Holden et al. (2018) with a PLASIM-GENIE ensemble the cloud back scattering range ($tswr_2$) parameter showed a correlation coefficient of -0.37 with PI and -0.01 with ECS. Therefore, to reduce the PI to normal levels without affecting the ECS, we set up the mentioned parameter $tswr_2$. The value of all the parameters changed to obtain the differed ECS are listed in Table. 2.

Table 2. Model Parameters modified and their values for the different ECS

Parameter	Standard	Enhanced	Extreme
k_{cont}	0.04	0.1	0.1
rh_c	0.85	0.85	0.93
$tswr_2$	0.048	0.048	0.05
maxalbice	0.7	0.7	0.75

2.5 Model diagnostics

In this section, we introduce the model variables used and how we transformed them to compute more complex ones also needed for the analysis.

PLASIM-GENIE returns yearly output of a list of variables in two different files coming from the named modules (i.e. PLASIM, GOLDSTEIN). From PLASIM we used the following atmospheric variables: surface temperature, vertically integrated specific humidity, top of the atmosphere net solar radiation, top of the atmosphere net thermal radiation, surface solar upward and surface albedo and from GOLDSTEIN the ocean variables we used are: Atlantic meridional streamfunction, zonal velocity, salinity, temperature, surface evaporation, precipitation, river runoff and sea ice freshwater input.

GMST, global mean albedo, global mean specific humidity and global mean SST are obtained as an area-wise average of the variables: surface temperature, surface albedo, vertically integrated specific humidity and the uppermost layer of ocean temperature. SST is also averaged over the Atlantic at 58ºN as an indicator of North Atlantic SST. OHC is calculated as the product of temperature, depth, seawater density, seawater specific heat capacity and the area of each ocean grid cell.

AMOC is evaluated in two different ways: (i) with the AMOC strength, defined as the maximum value of the Atlantic meridional streamfunction northern than 20ºN and deeper than 500m; (ii) the Atlantic meridional streamfunction cross-section.

To evaluate the response to emission reduction we use the slope after emission reduction. This is calculated for both, GMST and AMOC strength with a linear regression starting from the year with the maximum value of GMST (Fig. B3b). This value is found some years after t_s and is estimated using a 5th-degree polynomial fit of the GMST (Fig. B3a). By computing the slope from the maximum GMST, we neglect the GMST response lag found by Boucher et al. (2012), allowing us to analyse better additional dependencies. The slopes obtained for GMST response are also analysed in additional figures, with the ratio

GMST/CO_2 concentration, this is computed dividing the slope in GMST response by the slope in CO_2 concentration reduction for the different t_s, the values of these slopes are listed in Table. A1.

Integrated surface freshwater flux over the Atlantic is computed as the sum of precipitation, runoff and sea ice freshwater input minus evaporation and was integrated over the North Atlantic northern than 20ºN (Fig. B5). We compute this variable from this latitude to avoid taking into account the intertropical convergence zone (ITCZ), as this rises the freshwater flux one order of magnitude, hiding freshwater flux anomalies happening in the North Atlantic. To evaluate the freshwater influx as a forcing agent Gregory et al. (2003) evaluated the yearly accumulated amount from 35ºN to the north.

The last variable we define is the freshwater input into the North Atlantic by the AMOC. This is evaluated with Σ, a variable defined by Dijkstra (2007) and was found to be a good indicator in determining whether AMOC is in a multiple equilibria (ME) regime or not. When $\Sigma < 0$ the AMOC is found in the ME regime and is exporting freshwater out of the North Atlantic.

To deduce Σ, we first introduce zonal mean velocity $\bar{v}$:

$$\bar{v} = \int v \, cos\theta \, d\phi, \tag{8}$$

We also need to define the zonal salinity anomaly $\langle S \rangle$:

$$\bar{S} = \int S \, cos\theta \, d\phi \; ; \quad \langle S \rangle = \frac{\bar{S}}{\int cos\,\theta \, d\phi}, \tag{9}$$

These variables are computed for a given latitude θ. The overturning component of the freshwater import (M_{ov}) defined by De Vries and Weber (2005) is computed, according to:

$$M_{ov}(\theta) = -\frac{r_0}{S_0} \int_{S_\theta} \bar{v}(\langle S \rangle - S_0) dz. \tag{10}$$

Where S_0 and r_0 are the global average salinity (35 PSU) and the Earth radius. Last, to compute the net freshwater import into the North Atlantic we need to enclose the basin. The chosen latitudes for Northern (θ_N) and Southern (θ_S) boundaries are 58ºN and 30ºS (Fig. 4). We obtain the indicator Σ including both, the freshwater export at 30ºS and the freshwater input at 58ºN.

$$\Sigma(\theta_N, \theta_S) = M_{ov}(\theta_S) - M_{ov}(\theta_N) \tag{11}$$

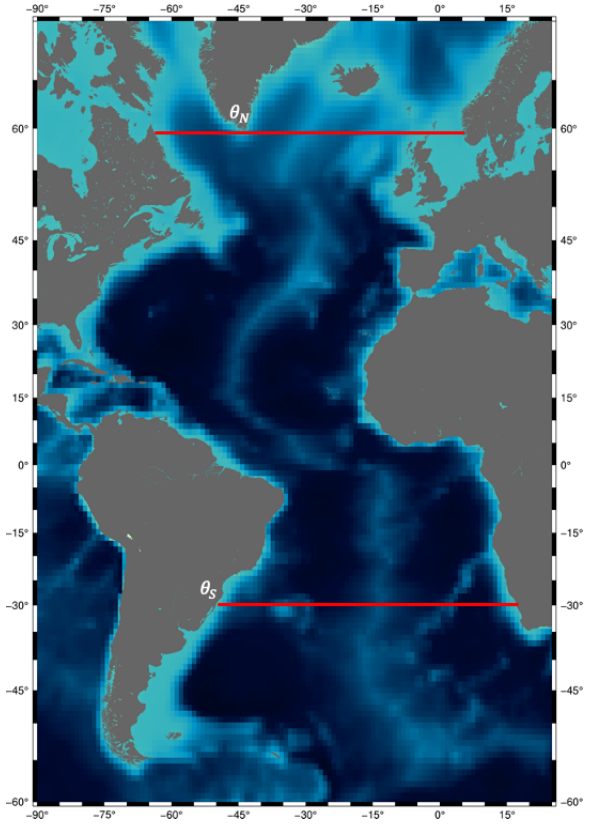

Figure 4. Map of the Atlantic showing the location of θ_N and θ_S.

Additionally, all the variables are filtered to smooth out noise and to give cleaner figures. AMOC strength, global mean albedo, Σ, Integrated surface freshwater flux over the Atlantic and SST in the North Atlantic are filtered with a 15-year run binomial filter. For the other variables a three year run binomial filter is also used, this time to slightly smooth the signals. The binomial filter used is defined to gradually reduce the number of years run near the boundaries.

3 Results

We plan to study the differences in the climate system response varying t_s and looking at the GMST to see the immediate response and the AMOC looking for deadlines to avoid tipping points. To test how the climate system responds to different t_s and ECS, we perform three sets of eight simulations with three different ECS and eight different t_s. All the simulations follow the CO_2 concentration from IRF_{CO_2} for RCP 8.5 emission scenario and the emission reduction pathways for different t_s as shown in Fig. 2b.

3.1 Basic variables

The increase in GMST for the different t_s on the three ECS is significantly different (Figs. B1a, B1c, B1e). The ΔT between t_s = 2020 and 2120 varies from 3ºC in the Standard ECS to, up to 4.5ºC in the Extreme ECS. With a maximum of 17.3, 19.5 and 20ºC GMST for the latest actions in the different ECS respectively.

In Figs. 5a, 5c, 5e we can see the decreasing slope of GMST after each t_s. In all three ECS, there is a non-monotonic behaviour for changes in t_s with notable differences between the different ECS. The effect of increasing the ECS is a higher variability for the GMST response on the different t_s, that becomes 2.5 and 4 times larger in the Enhanced and Extreme ECS than in the Standard. This increase represents a linear relationship between the ECS and the system response to emission reduction. All three ECS show a common trend of increase in the slope of the GMST response for later actions, faster responses of the system for later t_s. However, for t_s = 2120 the GMST response breaks the trend, with a slower GMST response in the Enhanced and Extreme ECS (Figs. 5c, 5e). This anomaly is exaggerated in the Extreme ECS with a positive slope in GMST after reducing emissions.

The behaviour of the GMST is also evaluated with GMST/CO_2 concentration ratios (Figs. 5b, 5d, 5f). In these figures, we can see two different trends. For the Standard ECS, the fastest response for ppm of carbon reduced lays in the earliest action (t_s = 2020), with decreasing speed for later t_s, while in the Enhanced and Extreme ECS, faster responses correspond to later actions. Again, this trend shows two anomalies with much slower responses (t_s = 2050 and 2120) on the Extreme ECS.

We also analyse other climate variables from the model (Figs. B1 and B2), global mean Sea Surface Temperature (SST), global mean albedo and global Ocean Heat Content (OHC). First, the SST which shows a smaller increment between the different t_s scenarios than GMST (Figs. B2a, B2c, B2e), with ΔT of 1.5, 2 and 2.5ºC for the three ECS. There is no difference in the reduced emissions response between SST and GMST. Both have the same behaviour, the correlation coefficient between them is 0.99, and there is no difference in the emission reduction response (Fig. B1). Second, the global mean albedo, it behaves very similarly for the three ECS. The difference between the first and last t_s is ~ 0.004 for all the ECS (Figs. B2b, B2d, B2f). Global mean albedo decreases progressively until (t_s), stabilizing its value right after. The response of the albedo to emission reduction is immediate; the albedo values stop decreasing as soon as the CO_2 concentration reaches maximum concentrations. For Enhanced and Extreme ECS, a small recovery arises after emission reduction for t_s later than 2070. The Enhanced ECS simulations have the lowest albedo values because the Extreme ECS included a slightly higher maximum sea-ice albedo (see in Table 1). Contrary to the previous variables, the OHC does not respond in the same time scale, not reaching equilibrium

before 2200 for any t_s later than 2050 in the Standard ECS, and not reaching it on any t_s for neither of Enhanced and Extreme ECS. The difference in OHC on the different ECS between t_s = 2020 and 2120 is of 300, 400 and 450 ZJ (Figs. B1b, B1d, B1f), with maximum OHC values at 2200 of 3230, 3650 and 3650 ZJ for the latest response t_s = 2120. Enhanced and Extreme reach the same maximum value. Although the Extreme ECS has a higher ECS, it has a slightly lower preindustrial temperature caused by the increase in $tswr_2$ value.

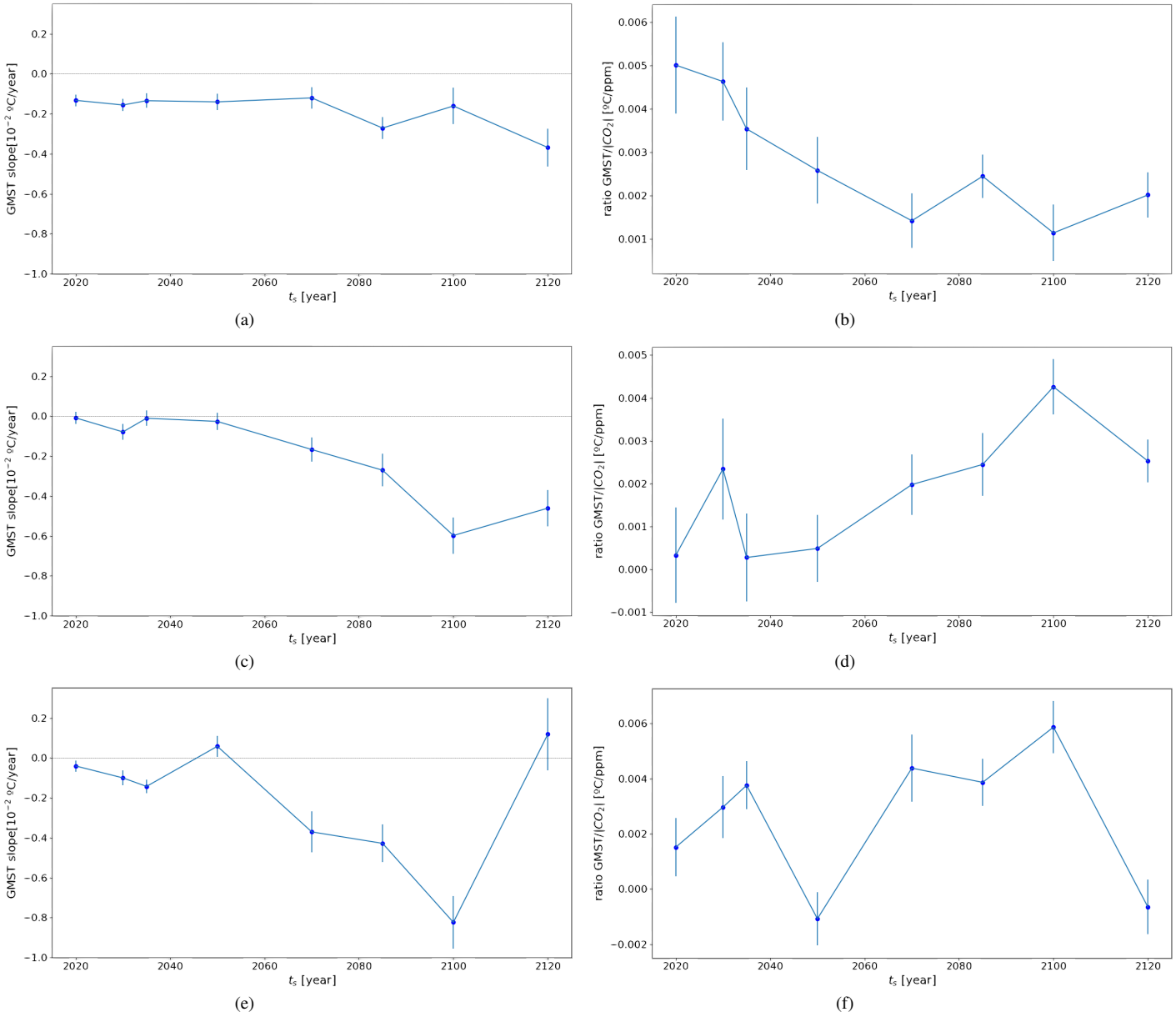

Figure 5. GMST response slope for different t_s (a,c,e) in Standard, Enhanced and Extreme ECS. GMST/CO_2 concentration slope for different t_s (b,d,f) in Standard, Enhanced and Extreme ECS.

3.2 AMOC

AMOC strength is plotted for the different t_s and ECS in Fig. 6. All the scenarios show a decrease in AMOC strength, which in most scenarios stabilizes after t_s but in others, continues to decrease reaching small values close to 0 Sv ($1Sv \equiv 10^6 m^3 s^{-1}$). For the Standard ECS (Fig. 6a), there is no great difference between the t_s scenarios; by 2200 the scenarios t_s = 2020 and t_s = 2085 differ by a 2 Sv difference for a 65 years action delay and about 4 Sv comparing t_s = 2020 with t_s = 2120. For the Enhanced and Extreme feedback scenarios (Figs. 6c and 6e) the result is significantly different. In Fig. 6c, Enhanced ECS, for actions later than $t_s = 2070$, the circulation keeps weakening after the emission reduction has started. For the two latest actions the minimum is not reached, not arriving to stable conditions inside the simulation time. In Fig. 6e, Extreme ECS, the AMOC does not reach equilibrium for any action taken later than $t_s = 2050$, for $t_s = 2070$ the AMOC seems to stabilize on $6Sv$ after emission reduction but it starts collapsing again 90 years later reaching $\approx 2Sv$ minimum.

Furthermore, we plot the AMOC pattern as the latitudinal section of the Atlantic meridional stream-function with a contour on 2200 for different t_s (2020, 2050, 2070 and 2100) and the different ECS (Fig. 7). The AMOC pattern conserves its characteristics between 2020 and 2200 in all the ECS with t_s = 2020. Later actions lead to less deep circulation with a net decrease of about 1000m in the Standard ECS and 2000m in the Enhanced ECS for actions preventing the collapse t_s = 2070 (Fig. 7b). In Figs. 7b, 7c, for Enhanced and Extreme ECS, the pattern of the AMOC suffers a drastic change for actions later than 2085 and 2050. For Enhanced ECS (Fig. 7b) we see that actions taken later than 2085 do not recover after emission reduction, and for Extreme (Fig. 7c) the deadline lies between 2070 and 2050, one collapsing while the other maintains the pattern after t_s. Collapsed scenarios exhibit negative circulation (southward) at $\approx$ 20ºN and $2000m$ depth.

The net freshwater input into the North Atlantic by AMOC is plotted in Fig. 6. In normal conditions (before 2100 for Enhanced, 2070 for Extreme ECS and all the t_s for Standard ECS) the net freshwater input by the AMOC is negative meaning that freshwater is being exported out of the Atlantic by the AMOC. Σ decreases in time for all the scenarios until it reaches a certain level (different for every t_s and ECS) and stabilizes. However, for the later actions in the Enhanced and Extreme ECS, the freshwater input values rise and become positive (Fig. 6d, 6f). The positive freshwater input matches all the scenarios with extreme AMOC weakening.

The integrated surface freshwater flux over the North Atlantic, shown in Figs. 8b, 8d and 8f, behaves in the same way for all the scenarios. For Standard ECS, which does not have any scenario with an AMOC collapse, the net freshwater influx remains negative with oscillating but stable values between -0.02 and 0 Sv, showing that there is more evaporation than precipitation integrating from 20ºN northwards. For Enhanced ECS, the result remains the same as for Standard ECS for all the scenarios with a $t_s \geq 2070$. However, all the scenarios that suffer an AMOC collapse plus t_s = 2085 exhibit positive anomalies of the freshwater influx rising the value to around 0.03 Sv. For Extreme ECS the integrated surface freshwater flux behaves in the same way as the Enhanced ECS, all the scenarios that have an AMOC collapse show a positive freshwater influx perturbation, this time up to 0.05 Sv. Overall the variability of this variable is $\approx$ 0.02 Sv in normal conditions and show anomalies of up to 0.07 Sv in AMOC collapsing conditions. These variations are indeed too small to be perceived when integrating this variable over the whole Atlantic as its value reaches $\approx$-0.3 Sv when we consider the equator and the ITCZ.

The analysis of the SST in the North Atlantic is performed to further analyse the behaviour of the AMOC. The value is obtained with the zonal average of North Atlantic SST at latitude 58ºN. In the Standard ECS (Fig. 8a), this variable does not show any uncommon behaviour for any t_s (i.e. higher SST for later actions with stabilization of the temperature after emission reduction). However, for the Enhanced and Extreme simulations (Figs. 8c and 8e), there are sharp decreases in SST of about 2ºC with a rate of 1ºC per decade for the later actions. These sharp decreases in the North Atlantic SST are found in t_s = 2100 and 2120 for the Enhanced ECS and $t_s \geq 2070$ for the Extreme ECS, with temperatures plunging between 1.5 and 3ºC.

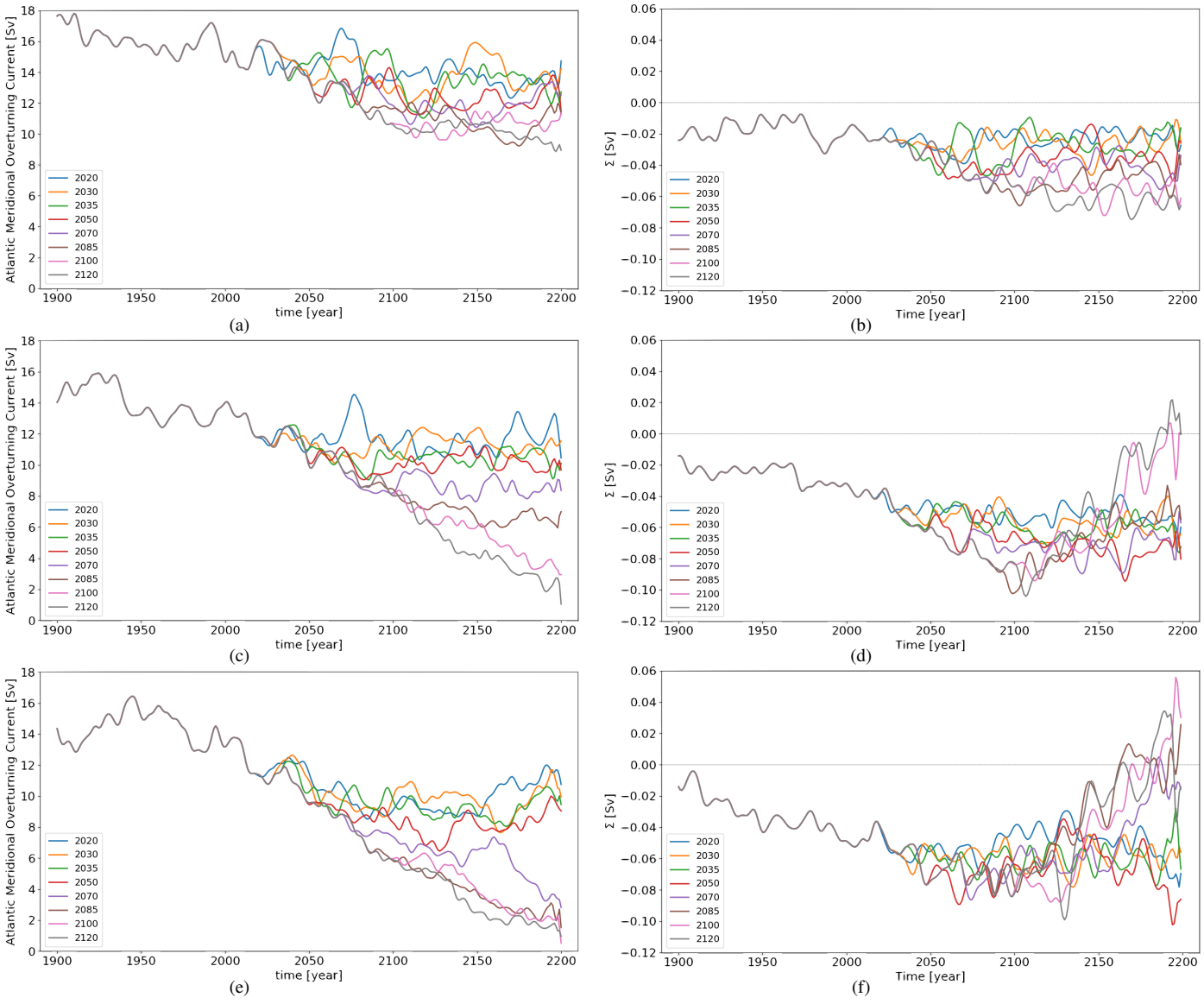

Figure 6. AMOC strength (a,c,e) in Standard, Enhanced, Extreme ECS for the different t_s. Freshwater input into the North Atlantic for the different t_s (b,d,f) with Standard Enhanced and Extreme ECS.

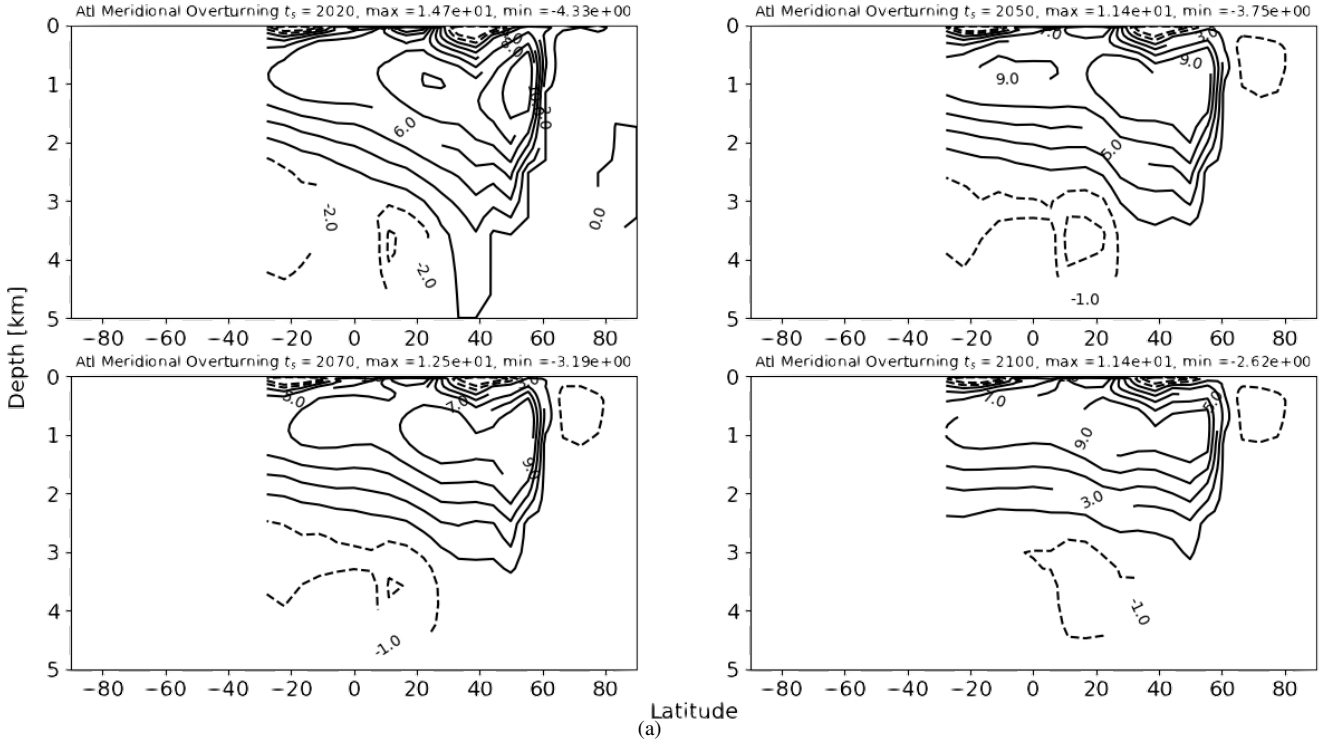
Atl Meridional Overturning t_s = 2020, max =1.47e+01, min =-4.33e+00
Atl Meridional Overturning t_s = 2050, max =1.14e+01, min =-3.75e+00
Atl Meridional Overturning t_s = 2070, max =1.25e+01, min =-3.19e+00
Atl Meridional Overturning t_s = 2100, max =1.14e+01, min =-2.62e+00
Depth [km]
Latitude

(a)

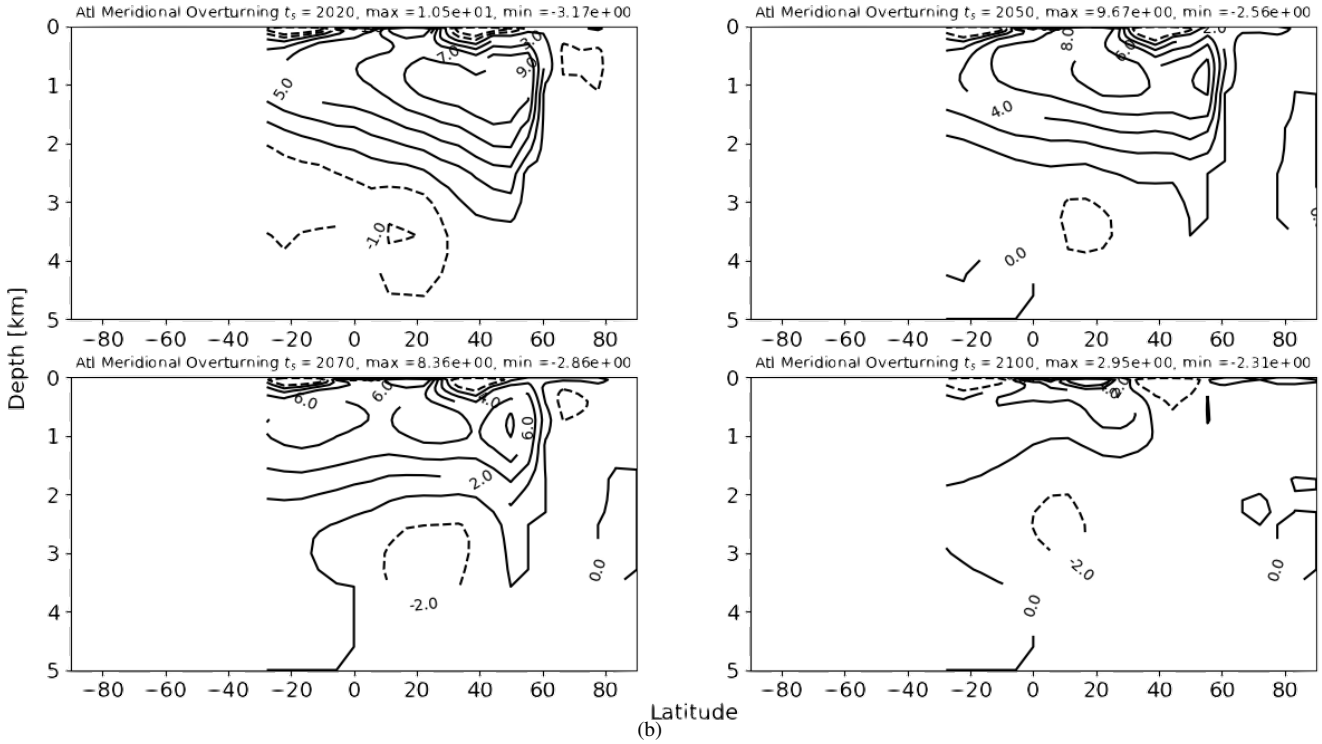
Atl Meridional Overturning t_s = 2020, max =1.05e+01, min =-3.17e+00
Atl Meridional Overturning t_s = 2050, max =9.67e+00, min =-2.56e+00
Atl Meridional Overturning t_s = 2070, max =8.36e+00, min =-2.86e+00
Atl Meridional Overturning t_s = 2100, max =2.95e+00, min =-2.31e+00
Depth [km]
Latitude

(b)

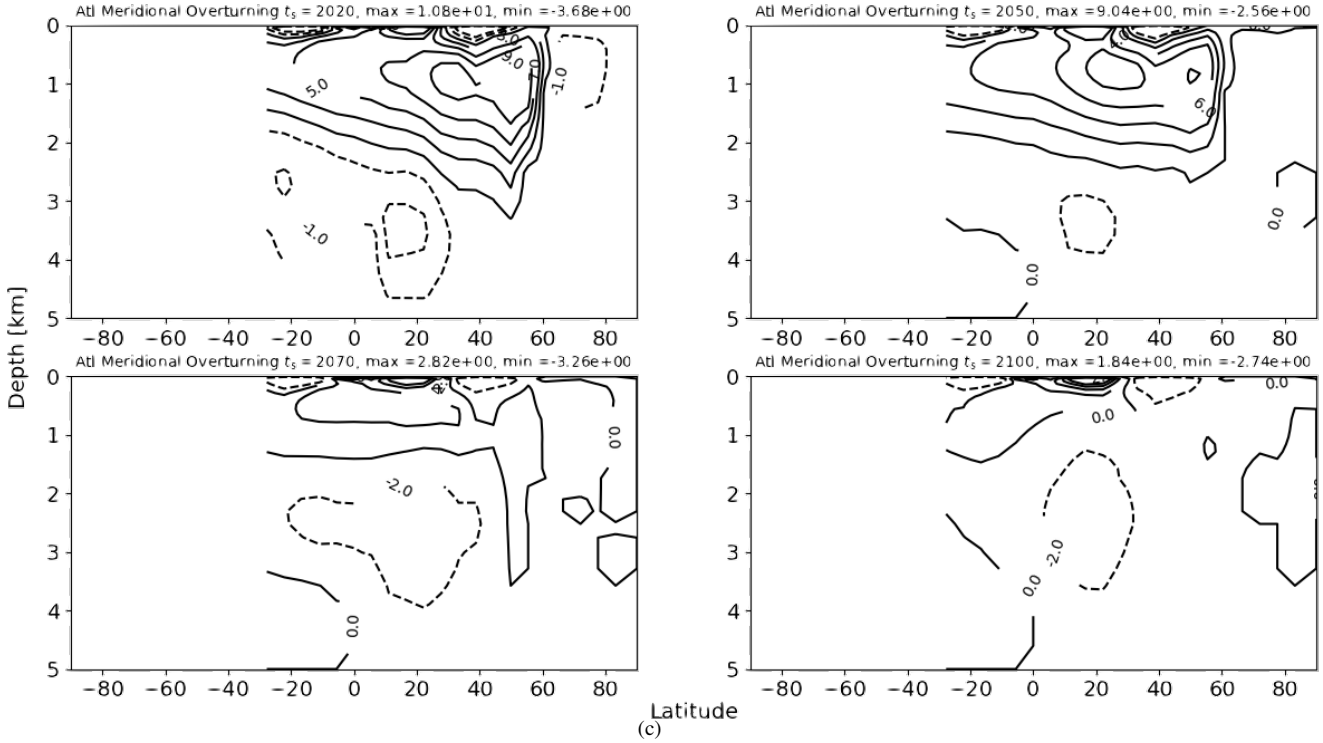

(c)

Figure 7. AMOC pattern on 2200 for different t_s years: 2020 (upper left), 2050 (upper right), 2070 (lower left), 2100 (lowe right) for (a) Standard, (b) Enhanced, (c) Extreme ECS

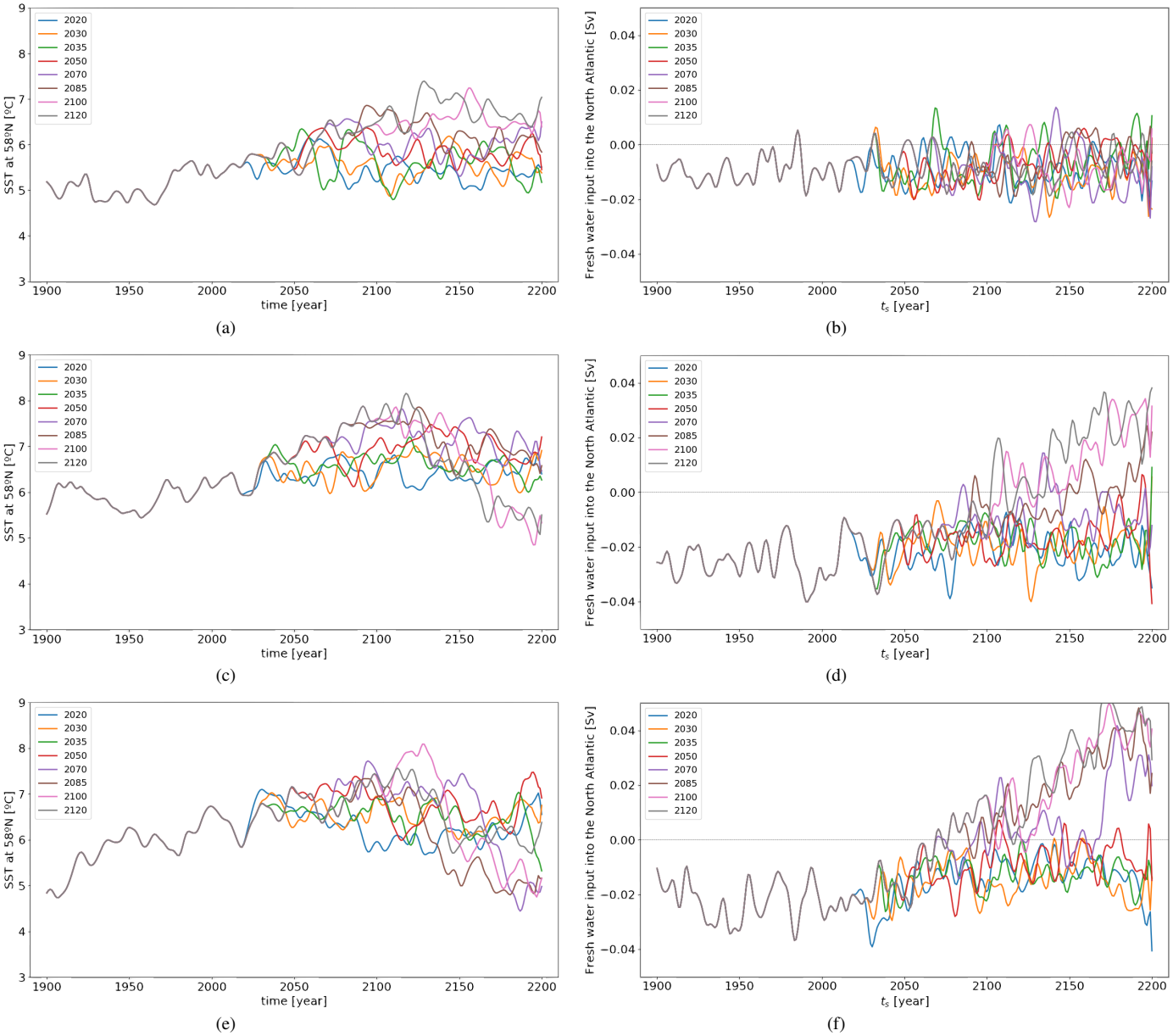

Figure 8. SST in the North Atlantic at latitude 58ºN for the different t_s (a,c,e) in Standard, Enhanced and Extreme ECS. Integrated surface freshwater flux over the North Atlantic for different t_s (b,d,f) in Standard, Enhanced and Extreme ECS.

3.3 GMST-AMOC correlation

The cross correlation between GMST anomalies and AMOC strength anomalies is obtained computing the ordinary least squares linear regression (OLS: using statsmodels package in Python) to explain the anomalies found in the GMST response to emission reduction (Fig. 5). This correlation shows a clear positive relation between GMST and AMOC strength in all scenarios with a sharp change in the AMOC strength (Fig. 9), for t_s = 2100 and 2120 for Enhanced ECS (OLS, β = 0.08ºCSv^{-1}, $r = 0.75$, $p = 1.69e-22$) and t_s = 2050, 2070, 2085 and 2100 for Extreme ECS (OLS, β = 0.1ºCSv^{-1}, $r = 0.8$, $p = 5.1e-82$).

The same test is performed considering all scenarios (Fig. B4) and the result shows a smaller but still significant correlation between GMST anomalies and AMOC anomalies (OLS, β = 0.025ºCSv^{-1}, $r = 0.25$, $p = 2.95e-13$) for Standard ECS, (OLS, β = 0.029 ºCSv^{-1}, $r = 0.25$, $p = 2.24e-13$) for Enhanced ECS and (OLS, β = 0.07 ºCSv^{-1}, $r = 0.59$, $p = 1.79e-80$) for Extreme ECS. The highest correlation is found in the Extreme ECS because it has more scenarios collapsing, which have a much higher correlation.

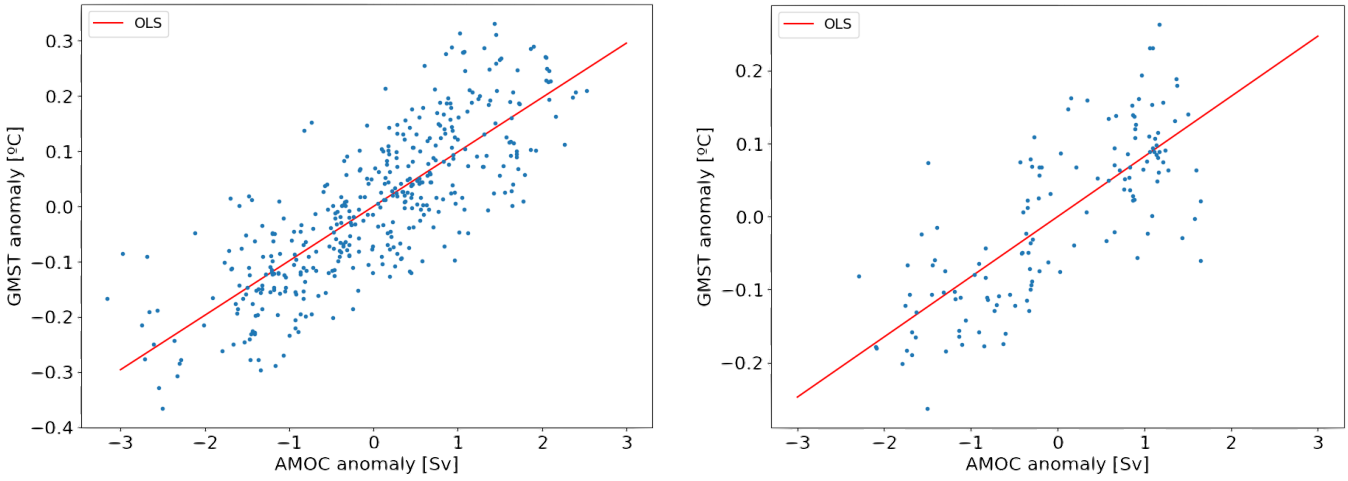

Figure 9. Ordinary Least Square linear regression for GMST anomaly vs AMOC anomaly for scenarios with an AMOC collapse (a) for Extreme ECS, (b) for Enhanced ECS.

Furthermore, analysing the AMOC strength response to emission reduction (Fig. 10), computed in the same period that GMST slope is calculated, allow us to clarify the behaviour of the GMST to emission reduction, even on the scenarios without a rapid variation of the AMOC. For the Standard ECS, the AMOC response appears to follow a multidecadal variability showing that the initial conditions of the AMOC strength at t_s might determine the slope after t_s. For t_s = 2120, there is a more negative GMST response because the AMOC keeps weakening after t_s, although not at a rapid pace. For Enhanced and Extreme ECS we see that the multidecadal variability still domains the resulting slope for all the scenarios in which the AMOC does not collapse. The effect of AMOC collapsing is a strong negative slope of the AMOC strength response, as expected. The latest action, t_s = 2120, for Enhanced and Extreme ECS shows a decrease in the slope strength when comparing to earlier

actions with AMOC collapse. By comparing Fig. 10 with Figs. 5a, 5c and 5e, we can relate the AMOC variability to GMST response anomalies. For example, we find a very clear GMST response anomaly on t_s =2085 for the Standard ECS, (Fig. 5a). The faster response of the GMST seems to follow the negative slope found in the AMOC (Fig. 10a). This relationship between negative (positive) slopes in the AMOC and faster (slower) responses of the GMST holds for all the anomalies found in all the scenarios (Figs. 5a, 5c and 5e).

All the scenarios that suffer a rapid change in AMOC strength after emission reduction show a high positive correlation between AMOC strength and GMST anomalies, with the only exception of t_s =2120 on Extreme ECS. Under growing CO_2 emissions scenarios, there is a negative correlation between GMST and AMOC, as positive anomalies in the GMST weaken the AMOC strength. However, in the emission reduction scenarios, there is a positive correlation between the AMOC and GMST. Stolpe et al. (2018) found this correlation examining the AMOC multidecadal variability effect on global temperatures. The impact of AMOC strength on GMST appears when an AMOC weakening leads to a smaller heat transport to high latitudes in the Atlantic increasing the Atmosphere-Ocean Heat transfer in this region and directly affecting on GMST.

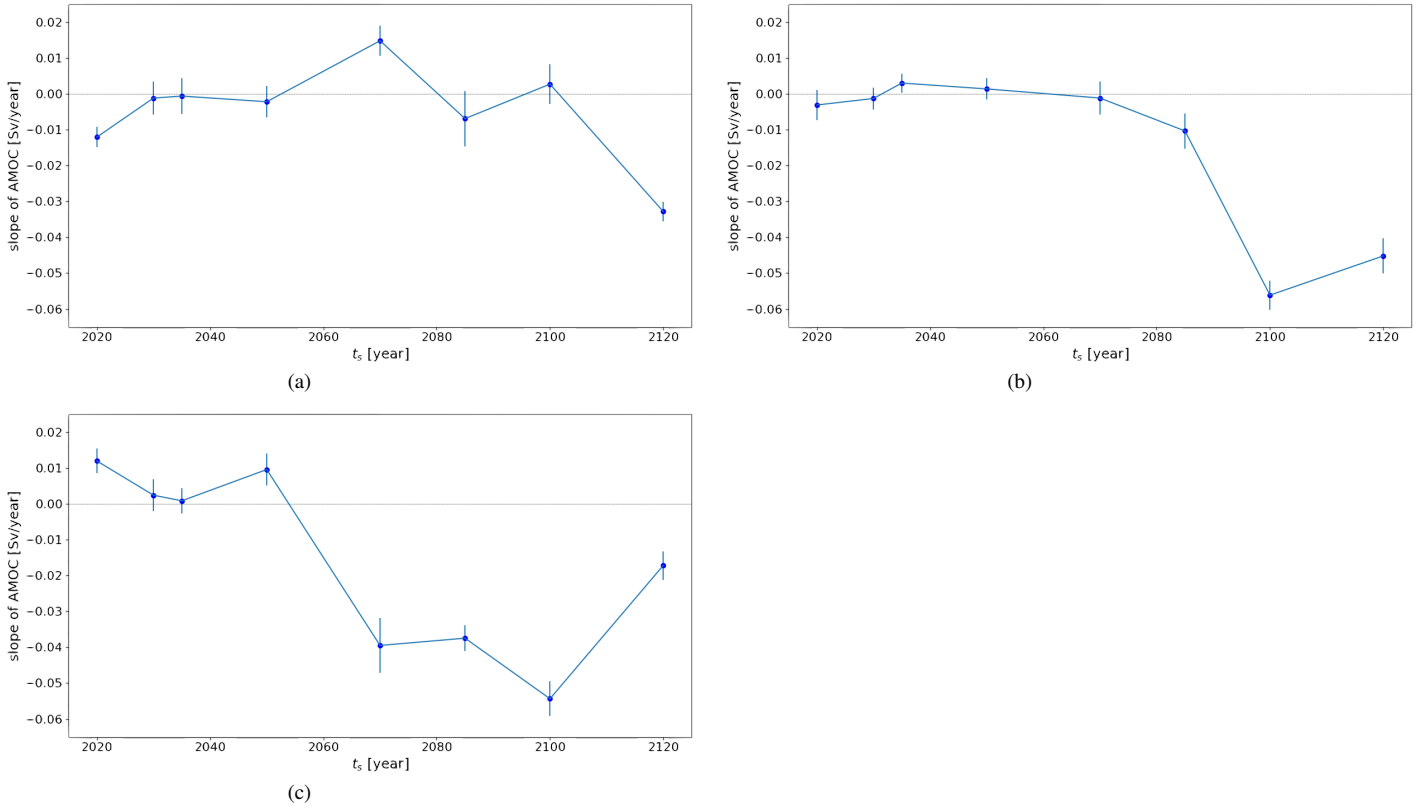

Figure 10. AMOC strength response slopes to emission reduction computed on the same period as Fig. 5 for different t_s, in Standard ECS (a), Enhanced ECS(b), Extreme ECS (c)

4 Discussion and Conclusions

Using a series of simulations from an intermediate complexity atmosphere and ocean model, we test the response of the earth system to emission reduction scenarios for different t_s and a range of ECS (2.77-4.5ºC). We look for non previously found dependencies of the GMST response on the time of starting emission reduction. To do so, we neglect the time lag in GMST reduction found by Boucher et al. (2012), computing the slope after the time lag. However, the differences found in GMST response are not large enough for the tested t_s to imply an advantage against an earlier action in the short-mid term for any ECS.

On the other hand, for larger ECS the system reaches tipping points inside the simulation run time, giving us a range of deadlines to avoid the AMOC collapse. These deadlines strongly depend on the ECS of the system, appearing earlier for higher ECS scenarios. In our study, we consider three cases inside the CMIP6 estimated ECS (Zelinka et al., 2020), but the collapse might happen earlier for the highest estimations of ECS predicted by CMIP6.

4.1 GMST response to emission reduction

The results show a highly variable response of the surface temperature to emission reduction for the different scenarios and ECS. There is a substantial increase in the variability of the GMST response between the different ECS, which is 2.5 and 4 times more variable for the stronger ECS simulations. These ECS are only 1ºC and 1.9ºC higher than the Standard ECS, making a linear relationship between the ECS and the variability of the GMST response. Despite the variability in the GMST response, there is a common trend for all our ECS; the temperature response is larger for later responses with emission reduction initial conditions of higher CO_2 concentration. But this trend might be explained by the behaviour of the emission reduction scenarios, as they take the same amount of time to reduce emissions to zero for all the t_s, with different initial CO_2 emission conditions. In Table. A1, we can see that for later t_s the slope of decreasing CO_2 concentration becomes larger, potentially forcing the temperature to reduce also faster. Therefore, to better evaluate the system response we analyse the ratio between temperature reduction and carbon concentration reduction (Figs. 5b, 5d, 5f). When we analyse the ratios, the GMST response loses the common trend for the different ECS, resulting in two different responses. The response of GMST to emission reduction scenarios depends on the actual strength of the climate feedbacks.

For weaker feedbacks simulations (e.g. Standard ECS), the GMST response to CO_2 concentration reduction is faster for the earliest action. This is due to the smaller effect of CO_2 concentration on GMST in this scenario. The initial conditions of the system at t_s dominate the emission reduction response rather than the slope of decreasing CO_2 concentration after t_s. Consistent with (Chen and Tung, 2018), we observe that on Standard ECS, there is a faster emission reduction response in those scenarios where there is a stronger AMOC (earlier actions).

For stronger feedback simulations (i.e. Enhanced and Extreme ECS), the GMST response to CO_2 concentration reduction is faster in the later t_s scenarios. The slope of CO_2 concentration might dominate the GMST response, showing a common trend of increasing GMST response for larger CO_2 concentration decreasing slopes. However, we can also explain the faster response of the later actions with the collapsing AMOC found in these simulations, knowing that these scenarios showed

a strong positive correlation between AMOC strength and GMST, we can conclude that it is the AMOC collapsing what dominates this trend.

The AMOC-GMST correlation explains well the non-linear behaviour found in GMST response (Fig. 5). This non-linear behaviour appears to be a consequence of the AMOC state and variability. One of the bigger anomalies found in Fig. 5f is the negative value on t_s = 2050, here the positive GMST response of the system is a consequence of the AMOC variability. The local minimum in GMST in 2120, followed by a maximum on 2145 makes the GMST response slope to become positive after t_s. The pronounced bounce on temperature seems to be represented on other variables such as the global albedo with the inverse pattern or the SST with the same pattern. However, it is the AMOC strength that is directly affecting the global SST and GMST, as was also found by Stolpe et al. (2018). The GMST minimum found in 2120 matches the weakening of the AMOC in the period from 2095 to 2130, while the maximum in 2148 coincides with the AMOC strengthening found between 2130 and 2150.

In this study, a strong correlation between AMOC and GMST anomalies (Fig. 9) appears in those scenarios that present a substantial variation in the AMOC strength. Yet, the other scenarios still exhibit a smaller positive correlation (Fig. B4). When comparing Fig. 10 with Fig. 5 we can see that the velocity of GMST response to emission reduction, is influenced by the slope of the AMOC in that same period. Faster (slower) responses for scenarios with more negative (positive) slopes in the AMOC.

The other anomalies such as t_s = 2085 for Standard ECS and t_s = 2030 for the Enhanced ECS with positive anomalies in the ratio GMST/CO_2 concentration, correspond to more negative values in the AMOC slope for that same period. The opposite effect is also found for t_s = 2120 in both Extreme and Enhanced ECS. Both show a less negative slope in AMOC than the earlier actions, reducing the GMST response to emission reduction. This would suggest that the cooling effect of AMOC collapsing is a transient effect on GMST. When AMOC collapses the net effect on GMST is cooling, but after a given time, the now collapsed state of the AMOC might reduce the GMST response to emission reduction. This hypothesis is consistent with the faster response for earlier actions for Standard ECS, when AMOC strength is in equilibrium the GMST response is faster (slower) for a stronger (weaker) AMOC. One example is the latest action (t_s = 2120) for Extreme ECS, where the system became response-less to emission reduction. In this scenario, the AMOC collapse happens before the GMST maximum is reached, leaving the system with an emission reduction response with the AMOC in a collapsed state. Although the atmosphere shows a transient cooling when AMOC collapses, the atmosphere seems to cool down more efficiently with a strong AMOC. Consistent with this hypothesis, Chen and Tung (2018) linked past warming episodes with periods of weaker AMOC.

4.2 AMOC Collapse

The possibility of AMOC collapsing might have been overlooked in CMIP5 with the existence of salinity bias in the North Atlantic (Liu et al., 2017). This bias is preventing the AMOC to collapse in the models. They found that the AMOC collapsed 300 years after doubling CO_2 concentration in a corrected model. Furthermore, they used the same criteria described by Dijkstra (2007) as a stability indicator, finding that the AMOC collapses when Σ starts to rise from negative values and eventually become positive. This is consistent with all our collapsing scenarios.

The AMOC is part of the global thermohaline circulation, this is driven by salinity and temperature gradients between low and high latitudes. Lower temperatures and higher salinity in the higher latitudes (fed by evaporation and sea-ice formation) force the circulation. In Dijkstra (2005), the salt advection feedback introduces the existence of multiple equilibria regime in the AMOC. For that reason, it is crucial to evaluate the saltwater budget in the North Atlantic, Σ is used as an indicator of ME regime in the AMOC (Dijkstra, 2007).

In all the tested ECS, the negative values of Σ indicate that the AMOC is found in a ME regime (Dijkstra, 2007; Liu et al., 2017), where it is susceptible to fall into a collapsed state under a given freshwater input perturbation. For $\Sigma < 0$, in a global warming scenario, the AMOC weakening decreases the freshwater exported out of the North Atlantic by the AMOC. The reduction in freshwater exported would lead to freshwater accumulation in the North Atlantic further weakening the AMOC, resulting in a collapse. In our results, values of Σ decrease in time, meaning an increase of freshwater exported out of the Atlantic. For all the scenarios that exhibit a collapse in the AMOC strength, Σ shows a growing trend towards positive values. This trend indicates a reduction in the freshwater exported by the AMOC. Once the freshwater divergence starts to weaken, the collapse forced by the salt advection feedback is inevitable. In six scenarios Σ reached positive values, indicating that they have entered a collapsed state of the AMOC (i.e. t_s = 2100, 2120 for Enhanced ECS and t_s = 2070, 2085, 2100, 2120 for Extreme ECS).

To analyse the origin of the AMOC collapse, we look into the integrated surface freshwater flux over the North Atlantic, searching for positive anomalies of freshwater input. Because $\Sigma < 0$, AMOC is found in a ME regime and a perturbation of the freshwater influx in the North Atlantic could cause a collapse. Positive freshwater anomalies in the North Atlantic can be caused by, for example, glaciers retreating (López-Gamundí and Buatois, 2010) or reduced evaporation (Van Aken, 2007). This last appears to be the reason for the anomaly found in all the collapsing AMOC scenarios, evaporation decreases when the SST plunges in all our collapsing scenarios, increasing the net freshwater influx in the North Atlantic.

The results from the integrated freshwater influx in the North Atlantic show that for all the scenarios with an AMOC collapse, a positive freshwater influx anomaly appears as a consequence of a weakened circulation. Remarkably, these positive perturbations of freshwater influx appear earlier than the AMOC collapse and could indicate that the t_s = 2085 scenario might collapse in a longer simulation. However, we also observe a common signal before the AMOC collapses, the retreat of the AMOC from high latitudes, and this symptom does not appear for t_s = 2085.

The negative anomaly in the SST on 58ºN for all the extremely weakened AMOC scenarios supports that the AMOC is in a collapsed state. Colder SST near the Pole would increase the AMOC strength by increasing the temperature gradient, enhancing the circulation in the normal AMOC state. But there is no response of the AMOC strength to this SST perturbation in any of the collapsed scenarios. On the contrary, the North Atlantic SST decline seems to be the source of reduced evaporation that translates into positive integrated freshwater influx, which is the perturbation that forces the system into a collapsed state.

The pattern of the AMOC in Fig. 7 gives a clear picture of the circulation weakening process. The circulation starts reducing its strength making the AMOC less deep. Then, it starts to retreat towards the equator, not reaching the high latitudes anymore, this step is crucial, once this happens the collapse is fed by the salt advection feedback. At last, we find southward circulation representing a different state of the AMOC, a collapsed state where the AMOC is importing freshwater instead of exporting it.

The AMOC collapse observed can be described with the following mechanism: (i) AMOC weakens as a response of global warming, fresher North Atlantic but not colder; (ii) AMOC retreats towards the equator due to the weakening; (iii) SST rapidly decreases in the North Atlantic as a consequence of the retreat; (iv) freshwater influx anomaly appears as a consequence of the reduced evaporation; (v) the amount of freshwater exported out of the Atlantic by the AMOC reduces as a consequence of the freshwater perturbation; (vi) freshwater perturbation grows, accumulates in the North Atlantic fed by the salt advection feedback; (vii) circulation is now driven by the salt gradient from lower salinity-density in the North Atlantic towards higher salinity-density in the equator.

On the other hand, no previous studies have found the AMOC to collapse under emission reduction scenarios. Urban and Keller (2010) suggests that an AMOC collapse in the 21st century is very unlikely (i.e. a probability less than 10%) and that this probability rises to up to a 35% by 2300 for a business-as-usual emissions scenario. However, they are following the IPCC assessment criteria (Alley et al., 2007) where the AMOC is defined to be in a collapsed state if the modelled AMOC strength is zero. Whereas in our study, we considered the AMOC to be in a collapsed state even when its strength is > 0 Sv. This is because of (i) the pattern observed (with opposite circulation), (ii) the unresponsive AMOC to ΔSST and (iii) the change in Σ from negative to positive values, which indicates that the system has entered a unique regime of AMOC collapsed state.

4.3 Conclusions

Our results support a possible dependency of the GMST on the AMOC variability and state in emission reduction scenarios, implying that to give an adequate estimation of the system response a complete evaluation of the AMOC must be performed. The results also support that small t_s differences can lead to GMST response differences. Nevertheless, in no case did a later action result in a lower GMST by the end of the 22nd century. Even if the simulations were performed with the same CO_2 concentration reduction scenario, instead of being time-dependent, the differences in t_s would not be enough to result in a substantial GMST response difference. That answers the question of what is the best year to start reducing emissions? The answer is the same for all the ECS; the soonest the best.

The AMOC prominence on emission reduction scenarios can be summarized in two points. (i) Variations in the AMOC have a direct effect on GMST response in emission reduction scenarios, with a faster (slower) response to emission reduction in weakening (strengthening) AMOC episodes; (ii) the efficiency of the atmosphere to cool down is enhanced by the existence of a stronger AMOC state, the GMST response to emission reduction is faster (slower) during stronger (weaker) states of the AMOC.

Furthermore, regarding tipping point deadlines, our model reaches an AMOC collapse in two of the three ECS tested. For any action later than 2050 when the ECS is 4.5ºC, and any t_s later than 2085 when the ECS is 3.7ºC. These results should call the attention of global governments and encourage them not to wait for any more than the strictly necessary to start implementing the emission reduction scenarios. However, taking into account that the results of this study could be model dependent, further research is needed to verify if the AMOC variability and state have the importance found in this study, testing the emission reduction scenarios in a high complexity fully coupled model with CO_2 concentrations reducing at the same pace.

References

Aengenheyster, M., Feng, Q. Y., Van Der Ploeg, F., and Dijkstra, H. A.: The point of no return for climate action. Earth System Dynamics., Earth System Dynamics, 9, doi:10.5194/esd-9-1085-2018, 2018.

Alley, R., Berntsen, T., Bindoff, N. L., Chen, Z., and Chidthaisong, A.: Climate Change 2007: The Physical Science Basis, Summary for Policymakers., IPCC, IPCC Secretariat, c/o WMO, 7bis, Avenue de la Paix, C.P. N 2300, 1211 Geneva 2, Switzerland, 2007.

Andrews, T., Gregory, J. M., Webb, M. J., and Taylor, K. E.: Forcing, feedbacks and climate sensitivity in CMIP5 coupled atmosphere-ocean climate models, Geophysical Research Letters, 39, doi:10.1029/2012GL051607, 2012.

Archer, D., Eby, M., Brovkin, V., Ridgwell, A., Cao, L., Mikola-jewicz, U., Caldeira, K., Matsumoto, K., Munhoven, G., Montenegro, A., and Tokos, K.: Atmospheric Lifetime of Fossil Fuel Carbon Dioxide., Annu. Rev. Earth Planet. Sci., 37, 117–134, doi:10.1146/annurev.earth.031208.100206, 2009.

Barnett, T. P., Pierce, D. W., and Schnur, R.: Detection of anthropogenic climate change in the world's oceans, Science, 292, 270–274, doi:10.1126/science.1058304, 2001.

Boucher, O., Halloran, P., Burke, E., Doutriaux-Boucher, M., Jones, C., Lowe, J., Ringer, M., Robertson, E., and Wu, P.: Reversibility in an Earth System model in response to CO2 concentration changes., Environmental Research Letters, 7, 024 013, doi:10.1088/1748-9326/7/2/024013, 2012.

Chen, X. and Tung, K.-K.: Global surface warming enhanced by weak Atlantic overturning circulation, Nature, 559, 387–391, doi:10.1038/s41586-018-0320-y, 2018.

Clarke, L., Edmonds, J., Jacoby, H., Pitcher, H., Reilly, J., and Richels, R.: Scenarios of greenhouse gas emissions and atmospheric concentrations, US Department of Energy Publications, https://digitalcommons.unl.edu/usdoepub/6, 2007.

Commission, E. and Agency, D. C. A. E. E.: Annual European Union greenhouse gas inventory 1990–2018 and inventory report 2020, UNFCCC Secretariat, https://www.eea.europa.eu/publications/european-union-greenhouse-gas-inventory-2020, 2020.

De Vries, P. and Weber, S. L.: The Atlantic freshwater budget as a diagnostic for the existence of a stable shut down of the meridional overturning circulation, Geophysical Research Letters, 32, doi:10.1029/2004GL021450, 2005.

Dijkstra, H. A.: Nonlinear physical oceanography: a dynamical systems approach to the large scale ocean circulation and El Nino, vol. 28, Springer Science & Business Media, 2005.

Dijkstra, H. A.: Characterization of the multiple equilibria regime in a global ocean model, Tellus A: Dynamic Meteorology and Oceanography, 59, 695–705, doi:10.1111/j.1600-0870.2007.00267.x, 2007.

Edwards, N. R. and Marsh, R.: Uncertainties due to transport-parameter sensitivity in an efficient 3-D ocean-climate model, Climate dynamics, 24, 415–433, doi:10.1007/s00382-004-0508-8, 2005.

Fraedrich, K., Kirk, E., Luksch, U., and Lunkeit, F.: The portable university model of the atmosphere.(PUMA):Storm track dynamics and low-frequency variability, Meteorol. Z, 14, 735–745, doi:10.1127/0941-2948/2005/0074, 2005.

Fujino, J., Nair, R., Kainuma, M., Masui, T., and Matsuoka, Y.: Multi-gas mitigation analysis on stabilization scenarios using AIM global model, The Energy Journal, doi:10.5547/ISSN0195-6574-EJ-VolSI2006-NoSI3-1, 2006.

Gregory, J., Saenko, O., and Weaver, A.: The role of the Atlantic freshwater balance in the hysteresis of the meridional overturning circulation, Climate Dynamics, 21, 707–717, doi:10.1007/s00382-003-0359-8, 2003.

Gregory, J. M., Ingram, W., Palmer, M., Jones, G., Stott, P., Thorpe, R., Lowe, J., Johns, T., and Williams, K.: A new method for diagnosing radiative forcing and climate sensitivity, Geophysical research letters, 31, doi:10.1029/2003GL018747, 2004.

Grubb, M., Vrolijk, C., Brack, D., Forsyth, T., Lanchbery, J., and Missfeldt, F.: The Kyoto Protocol: a guide and assessment, vol. 10, Royal Institute of International Affairs London, 1999.

Holden, P. B., Edwards, N. R., Garthwaite, P. H., Fraedrich, K., Lunkeit, F., Kirk, E., Labriet, M., Kanudia, A., and Babonneau, F.: PLASIM-ENTSem v1.0: a spatio-temporal emulator of future climate change for impacts assessment, Geosci. Model Dev., 7, 433–451, doi:10.5194/gmd-7-433-2014, 2014.

Holden, P. B., Edwards, N. R., Fraedrich, K., Kirk, E., Lunkeit, F., and Zhu, X.: PLASIM–GENIE v1. 0: a new intermediate complexity AOGCM., Geoscientific Model Development, 9, 3347–3361, doi:10.5194/gmd-9-3347-2016, 2016.

Holden, P. B., Edwards, N. R., Ridgwell, A., Wilkinson, R., Fraedrich, K., Lunkeit, F., Pollitt, H., Mercure, J.-F., Salas, P., Lam, A., et al.: Climate–carbon cycle uncertainties and the Paris Agreement, Nature Climate Change, 8, 609, doi:10.1038/s41558-018-0197-7, 2018.

Joos, F., Roth, R., Fuglestvedt, J. S., Peters, G. P., Enting, I. G., Von Bloh, W., Brovkin, V., Burke, E. J., Eby, M., Edwards, N. R., Friedrich, T., Frölicher, T. L., Halloran, P. R., Holden, P. B., Jones, C., Kleinen, T., Mackenzie, F. T., Matsumoto, K., Meinshausen, M., Plattner, G., Reisinger, A., Segschneider, J., Shaffer, G., Steinacher, M., Strassmann, K., Tanaka, K., Timmermann, A., and Weaver, A. J.: Carbon dioxide and climate impulse response functions for the computation of greenhouse gas metrics: a multi-model analysis., Atmospheric Chemistry and Physics, 13, 2793–2825, doi:10.5194/acp-13-2793-2013, 2013.

Kheshgi, H., de Coninck, H., and Kessels, J.: Carbon dioxide capture and storage: seven years after the IPCC special report, Mitigation and adaptation strategies for global change, 17, 563–567, doi:10.1007/s11027-012-9391-5, 2012.

Le Quéré, C., Andrew, R. M., Friedlingstein, P., Sitch, S., Hauck, J., Pongratz, J., Pickers, P. A., Korsbakken, J. I., Peters, G. P., Canadell, J. G., et al.: Global carbon budget 2018, Earth System Science Data, 10, 2141–2194, doi:10.5194/essd-10-2141-2018, 2018.

Lenton, T. M., Held, H., Kriegler, E., Hall, J. W., Lucht, W., Rahmstorf, S., and Schellnhuber, H. J.: Tipping elements in the Earth's climate system, Proceedings of the national Academy of Sciences, 105, 1786–1793, doi:10.1073/pnas.0705414105, 2008.

Liu, W., Xie, S.-P., Liu, Z., and Zhu, J.: Overlooked possibility of a collapsed Atlantic Meridional Overturning Circulation in warming climate, Science Advances, 3, e1601 666, doi:10.1126/sciadv.1601666, 2017.

López-Gamundí, O. R. and Buatois, L. A.: Late Paleozoic glacial events and postglacial transgressions in Gondwana, vol. 468, Geological Society of America, 2010.

McManus, J. F., Francois, R., Gherardi, J.-M., Keigwin, L. D., and Brown-Leger, S.: Collapse and rapid resumption of Atlantic meridional circulation linked to deglacial climate changes, Nature, 428, 834–837, doi:10.1038/nature02494, 2004.

Millar, R. J., Nicholls, Z. R., Friedlingstein, P., and Allen, M. R.: A modified impulse-response representation of the global near- surface air temperature and atmospheric concentration response to carbon dioxide emissions., Atmospheric Chemistry and Physics, 17, 7213– 7228, doi:10.5194/acp-17-7213-2017, 2017.

Noël, B., van De Berg, W., Lhermitte, S., Wouters, B., Machguth, H., Howat, I., Citterio, M., Moholdt, G., Lenaerts, J., and van den Broeke, M. R.: A tipping point in refreezing accelerates mass loss of Greenland's glaciers and ice caps, Nature Communications, 8, 1–8, doi:10.1038/ncomms14730, 2017.

Ponomarev, Y. N., Solodov, A., Solodov, A., Petrova, T., and Naumenko, O.: FTIR spectrometer with 30 m optical cell and its applications to the sensitive measurements of selective and nonselective absorption spectra, Journal of Quantitative Spectroscopy and Radiative Transfer, 177, 253–260, doi:10.5194/amt-11-2159-2018, 2016.

Rahmstorf, S.: On the freshwater forcing and transport of the Atlantic thermohaline circulation, Climate Dynamics, 12, 799–811, 1996.

Rahmstorf, S., Crucifix, M., Ganopolski, A., Goosse, H., Kamenkovich, I., Knutti, R., Lohmann, G., Marsh, R., Mysak, L. A., Wang, Z., et al.: Thermohaline circulation hysteresis: A model intercomparison, Geophysical Research Letters, 32, doi:10.1029/2005GL023655, 2005.

Riahi, K., Rao, S., Krey, V., Cho, C., Chirkov, V., Fischer, G., Kindermann, G., Nakicenovic, N., and Rafaj, P.: RCP 8.5—A scenario of comparatively high greenhouse gas emissions., Atmospheric Chemistry and Physics, 109, 33–57, doi:10.1007/s10584-011-0149-y, 2011.

Rosenzweig, C., Karoly, D., Vicarelli, M., Neofotis, P., Wu, Q., Casassa, G., Menzel, A., Root, T. L., Estrella, N., Seguin, B., et al.: Attributing physical and biological impacts to anthropogenic climate change, Nature, 453, 353–357, doi:10.1038/nature06937, 2008.

Schneider, E. K., Kirtman, B. P., and Lindzen, R. S.: Tropospheric water vapor and climate sensitivity., Journal of the atmospheric sciences, 56, 1649–1658, 1999.

Stolpe, M. B., Medhaug, I., Sedláček, J., and Knutti, R.: Multidecadal variability in global surface temperatures related to the Atlantic Meridional Overturning Circulation, Journal of Climate, 31, 2889–2906, doi:10.1175/JCLI-D-17-0444.1, 2018.

Urban, N. M. and Keller, K.: Probabilistic hindcasts and projections of the coupled climate, carbon cycle and Atlantic meridional overturning circulation system: a Bayesian fusion of century-scale observations with a simple model, Tellus A: Dynamic Meteorology and Oceanography, 62, 737–750, doi:10.1111/j.1600-0870.2010.00471.x, 2010.

Van Aken, H. M.: The oceanic thermohaline circulation: An introduction, vol. 39, Springer Science & Business Media, 2007.

Van Vuuren, D. P., Den Elzen, M. G., Lucas, P. L., Eickhout, B., Strengers, B. J., Van Ruijven, B., Wonink, S., and Van Houdt, R.: Stabilizing greenhouse gas concentrations at low levels: an assessment of reduction strategies and costs, Climatic change, 81, 119–159, doi:10.1007/s10584-006-9172-9, 2007.

Williamson, M. S., Lenton, T. M., Shepherd, J. G., and Edwards, N. R.: An efficient numerical terrestrial scheme (ENTS) for Earth system modelling, Ecological Modelling, 198, 362–374, doi:10.1016/j.ecolmodel.2006.05.027, 2006.

World Energy Council: World Energy Resources, Tech. rep., World Energy Council, London, 2016.

Zelinka, M. D., Myers, T. A., McCoy, D. T., Po-Chedley, S., Caldwell, P. M., Ceppi, P., Klein, S. A., and Taylor, K. E.: Causes of higher climate sensitivity in CMIP6 models, Geophysical Research Letters, doi:10.1029/2019GL085782, 2020.

Appendix A: Tables

Table A1. The slopes of the decreasing concentration after t_s in ppm/year, the slopes for GMST response after t_s in K/year for the different ECS

t_s	Slope CO_2 concentration	GMST Standard	GMST Enhanced	GMST Extreme
2020	-0.264437	-0.001324	-0.000086	-0.000401
2030	-0.336308	-0.001556	-0.000787	-0.000998
2035	-0.379164	-0.001342	-0.000104	-0.001426
2050	-0.542064	-0.001401	-0.000263	0.000584
2070	-0.844337	-0.001203	-0.001670	-0.003701
2085	-1.105918	-0.002708	-0.002706	-0.004276
2100	-1.402509	-0.001606	-0.005975	-0.008232
2120	-1.823607	-0.003681	-0.004606	0.001188

Appendix B: Complementary figures

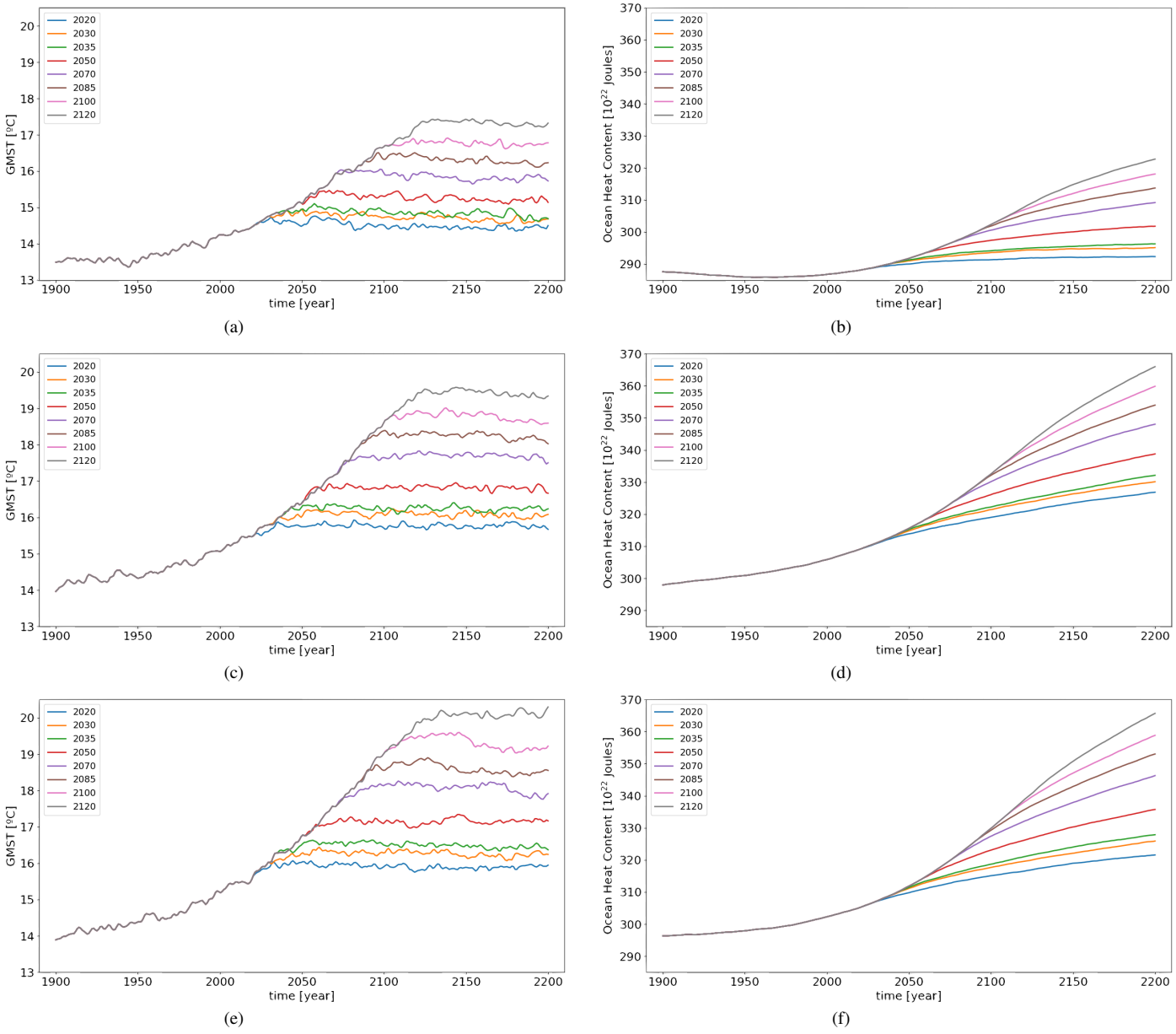

Figure B1. GMST on different t_s (a,c,e) in Standard, Enhanced, Extreme ECS. OHC for different t_s (b,d,f) in Standard Enhanced and Extreme ECS.

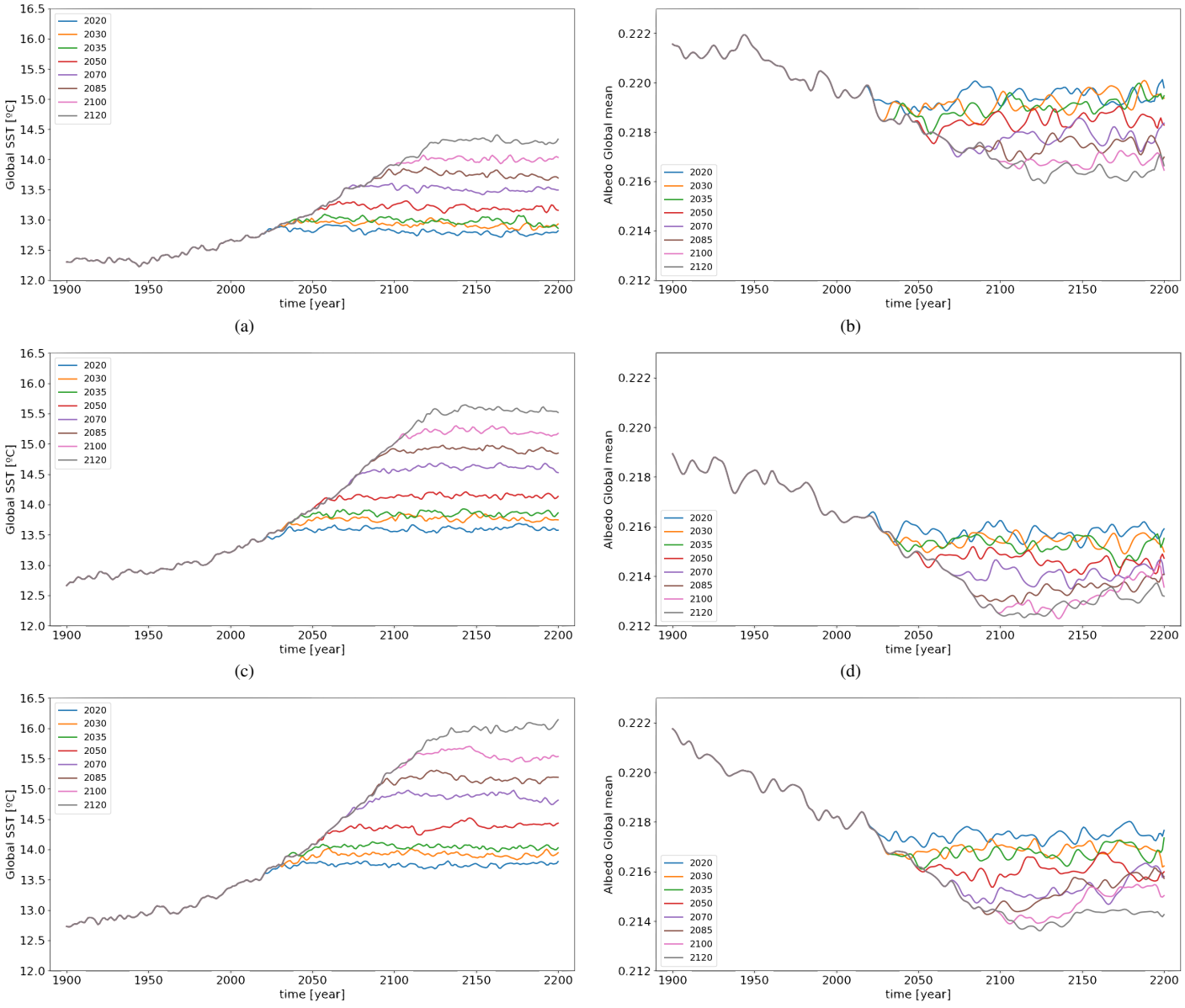

Figure B2. SST for different t_s (a,c,e) in Standard, Enhanced, Extreme ECS. Global mean albedo for different t_s (b,d,f) in Standard Enhanced and Extreme ECS.

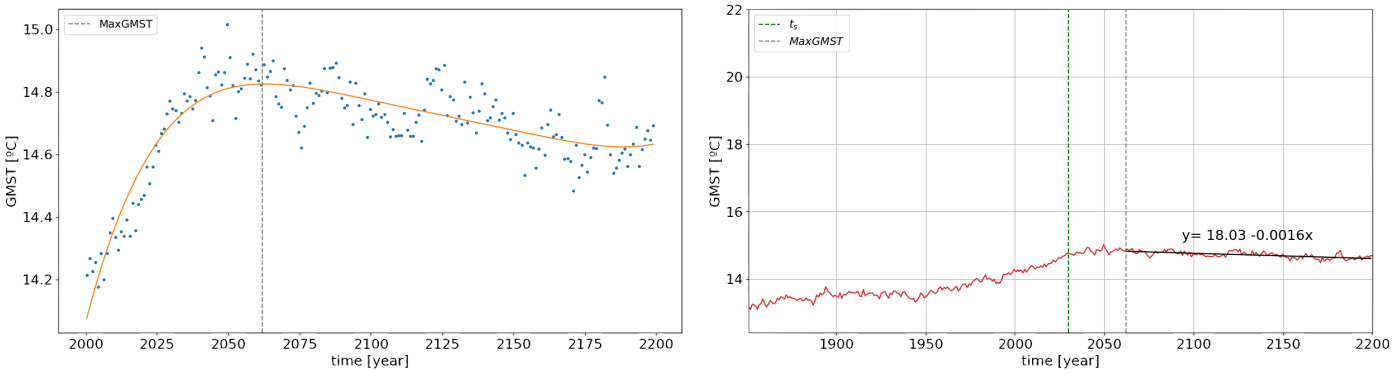

Figure B3. (a) Example of the 5th degree polynomial fit used to estimate the maximum GMST, (b) Slope estimation method used for Figs. 5 and 10, calculated with a linear regression.

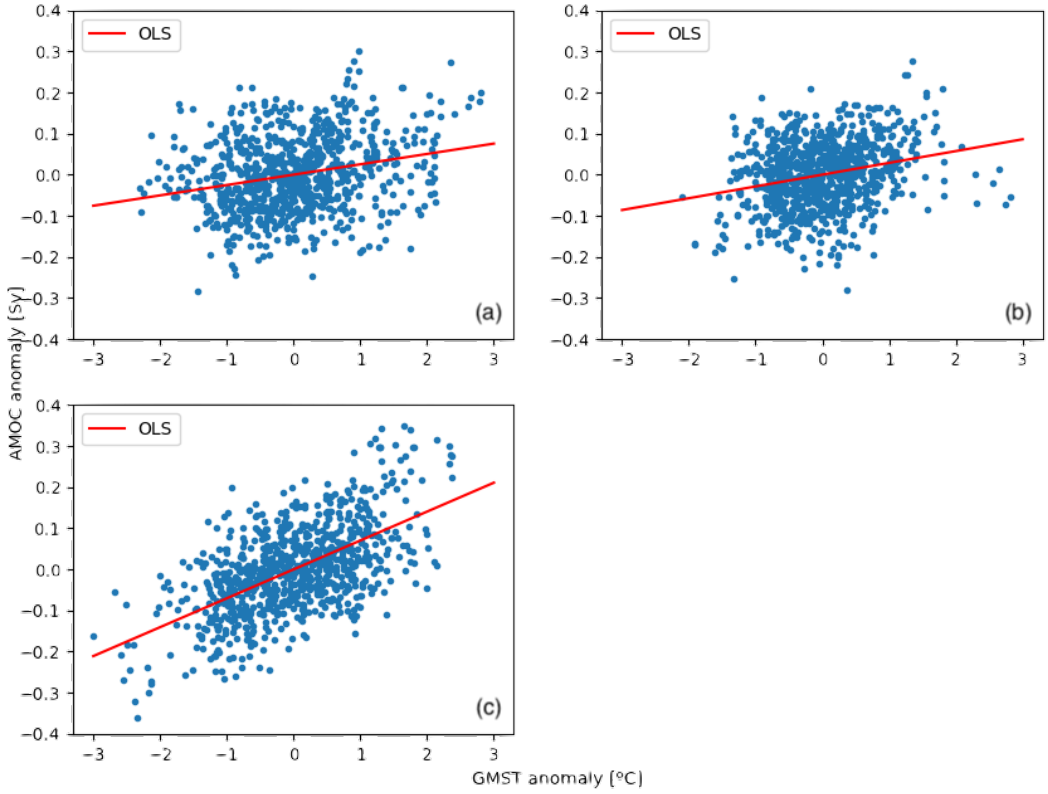

Figure B4. Ordinary Least Square linear regression for GMST anomaly vs AMOC anomaly for all the scenarios and the different ECS, (a) Standard, (b) Enhanced, (c) Extreme

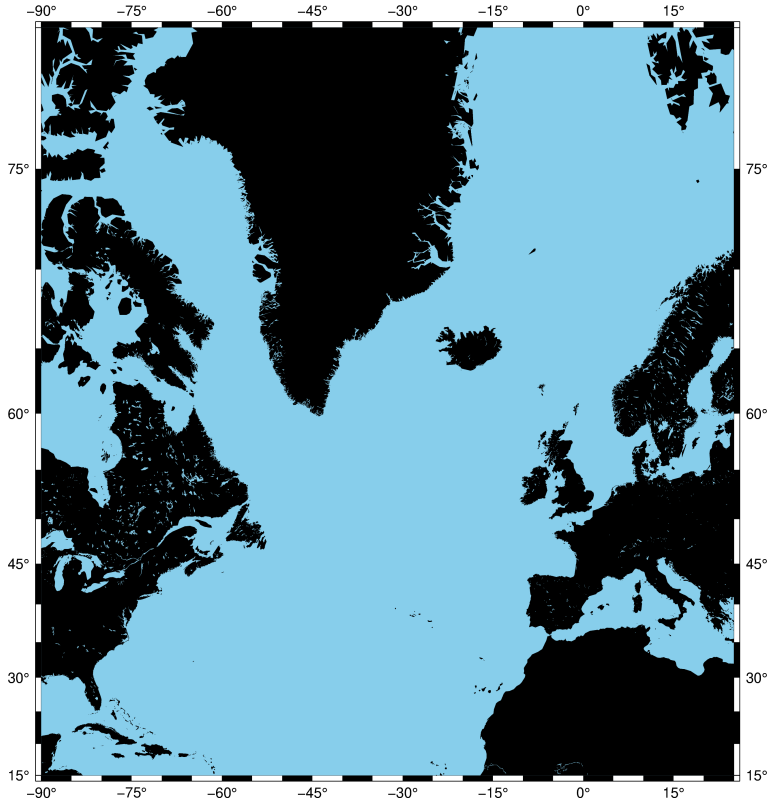

Figure B5. Area in the North Atlantic where the integrated surface freshwater flux over the North Atlantic is computed.